Macromolecules

Open Access
This article is licensed under CC-BY 4.0

pubs.acs.org/Macromolecules
Article

The Influence of Thermoreversible Diels–Alder Bonds on the Structure, Morphology, and Rheology of Recyclable Thermoplastic Polyurethanes

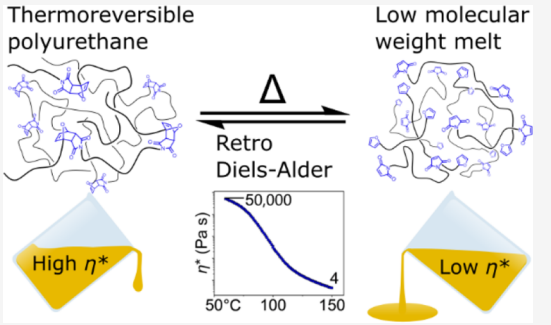
Thomas S. Jackson, Andrew T. Slark,* and Oleksandr O. Mykhaylyk*

Cite This: https://doi.org/10.1021/acs.macromol.6c01484

Read Online

ACCESS | Metrics & More | Article Recommendations | Supporting Information

ABSTRACT: Conventional thermoplastic polyurethanes (PU) are difficult to recycle due to their high melt viscosity. In this work, a semi-crystalline polyurethane comprising thermoreversible Diels–Alder (DA) cycloadducts in the backbone was prepared and compared to an analogue containing conventional butanediol (BDO) chain extender. The **DA-PU** was shown to successfully dissociate at high temperatures and reach a very low melt viscosity of 4 Pa.s. Isothermal crystallization experiments showed that the crystallization kinetics of **DA-PU** were strongly dependent on the melting temperature because of its dynamic molecular weight. SAXS and rheological measurements showed that **DA-PU** exhibited a more phase-mixed melt morphology than its **BDO-PU** analogue, which displayed distinct hard-soft segment phase separation. These morphological differences were reflected in the rheological measurements. Frequency sweep measurements showed that master curves could be constructed for **DA-PU** by time-temperature or time-molecular weight superposition. Kinetic and thermodynamic parameters E_a, $\Delta H^{\ominus}$ and $\Delta S^{\ominus}$ for the DA reaction were obtained from rheology and FTIR. The data shows that incorporating DA cycloadducts in thermoplastic polyurethanes provides a fundamental change to thermal properties, morphology, and rheology, suggesting a different paradigm for processability and properties.



■ INTRODUCTION

Polyurethanes (PU) are highly industrially relevant materials due to their many applications as coatings, adhesives, sealants and elastomers. Over 27 million tons of PU were sold in 2024, with market volume growth projected to continue over the rest of the decade.[1] Crosslinked PUs account for the majority of the market due to their excellent mechanical properties but they cannot be recycled due to their permanent network structures. Thermoplastic polyurethanes (TPUs) on the other hand can be mechanically recycled in principle, but the requirement for high temperatures and high shear during reprocessing causes thermo-mechanical degradation, which reduces mechanical properties and limits the applications of recycled TPUs, as well as the number of reprocessing cycles they can withstand.[2] Thus, the majority of PU waste is sent to landfill.[3] Mitigating this has been an area of significant environmental interest in recent years, with particular attention being placed in polymers containing covalent bonds which are reversible under a certain stimulus.[4] One such type of reaction which has been investigated is the thermally reversible Diels–Alder (DA) reaction between prepolymers terminated with maleimide dienophile groups and furan diene groups.[5−8] This DA reaction is a promising candidate in reversible polymer applications due to its facile 'click-chemistry' nature, commercially available feedstocks and mild retro Diels–Alder (rDA) dissociation reaction conditions. In principle, simply heating the material above 120 °C causes it to dissociate quickly, reducing its molecular weight to that of the prepolymer level. This process reduces the melt viscosity, facilitating recycling. Consequently, significant effort has been directed toward incorporating this chemistry into crosslinked networks containing dynamic bonds, known as Covalent Adaptable Networks (CANs).[9−12]

While crosslinked CANs have received much focus in recent years, there has been much less research into linear thermoplastic polymers comprising DA bonds in the polymer backbone.[13] TPUs are common in elastomer and adhesive applications, with debondable PU adhesives being a current subject of interest in polymer research.[14,15] Previous studies of linear DA TPUs have primarily focused on materials based on MDI, in which the hard segments are chain-extended through DA cycloadducts formed between maleimide and furan groups. These materials have

Received: May 27, 2026
Revised: September 4, 2026
Accepted: October 1, 2026

Downloaded from pubs.acs.org/mamobx/article-pdf/doi/10.1021/acs.macromol.6c01484/6895018/ma-2026-014843.pdf by guest on 04 November 2026

demonstrated strong mechanical properties, as evidenced by tensile and lap-shear testing. Following reprocessing by heating at 120–150 °C, near-complete recovery of both the DA bond concentration and molecular weight was observed after equilibration for 7 days under ambient conditions. The mechanical properties were also retained over several reprocessing cycles.[16,17] Since these materials can be reprocessed under relatively mild thermal conditions, the DA TPUs exhibited good chemical stability and retained their performance over repeated recycling cycles. These findings highlight DA TPUs as promising candidates for recyclable polyurethane materials. However, despite the demonstrated reversibility and mechanical robustness, the influence of DA cycloadduct formation on the molecular organization and structural morphology of polyurethane remains relatively unexplored. Du et al. investigated linear amorphous DA TPUs containing poly(butylene glycol), and used atomic force microscopy (AFM) to show the phase-separated morphology in the DA copolymer compared to its butanediol (BDO) chain-extended analogue.[8] In other work, Small-Angle X-ray Scattering (SAXS) data were obtained for poly(ε-caprolactone) (PCL) and poly(butadiene) based DA TPUs, and the presence of multiple scattering peaks indicated that a complex structural morphology was formed.[16,18]

It is well known that the structure, size and symmetry of the chain extender have an influence on the morphology and mechanical properties of polyurethanes,[19−24] as the chain extender influences the degree of hydrogen bonding between adjacent urethane groups. In general, small glycol molecules with an even number of methylene units (such as butanediol) are preferred.[25] It could be expected that use of a bulky tricyclic DA cycloadduct as a chain extender would have a significant effect on structural morphology and associated mechanical properties. Previous works on morphologies of PUs with bulky nonreversible chain extenders have shown mixed results,[23,26] and as such it is difficult to predict the effect that the DA cycloadduct would have on the resulting PU morphology when used as a chain extender.

Crystallinity in the soft segment (SS) has been shown to improve the low-temperature mechanical properties of TPUs with low hard segment (HS) content, shown by a drop in elastic modulus upon SS melting, as well as high elongation at break via tensile testing measurements.[27−31] Thus, the literature suggests that in the absence of HS crystallinity, SS crystallinity is the controlling factor over the strength of the material. Therefore, it is logical that SS crystallinity could be highly advantageous for materials such as DA TPUs, where the HS crystallization is likely to be hindered by the DA chain extender.

A thorough structural analysis was performed in the current work on a semicrystalline TPU containing highly asymmetric DA cycloadducts as chain extenders, including the evaluation of thermal properties, morphology and rheological behavior. These TPUs comprise chemical components that govern hydrogen bonding, crystallinity and dynamic molecular weight, resulting in highly tunable material properties suitable for reuse and reprocessing, with relevance to elastomer and adhesive applications. Accordingly, a thermally reversible TPU containing DA cycloadducts in the polymer backbone (referred to as **DA-PU**) was synthesized, containing poly(ε-caprolactone) polyol (referred to as **PCL-3k**) as the soft segment. A relatively high molecular weight grade of PCL polyol was chosen to ensure SS crystallinity which imparts mechanical strength.[17,18] 4,4′-methylene diphenyl diisocyanate (MDI) was chosen for the hard segment diisocyanate due to its high reactivity, low handling risk and low cost which makes it highly scalable and industrially relevant. **DA-PU** was then compared to an analogous material in which the Diels–Alder chain-extender was replaced with 1,4-butanediol (referred to as **BDO-PU**) as this is used as the primary chain extender in conventional TPUs. A direct and detailed comparison is made between the morphological and physical properties in these systems because of changes in the molecular architecture of the chain-extender. The effect of different components on the material structure was identified from a 'bottom up' approach, where the complexity of the system was increased incrementally. By each technique, the semicrystalline polyester structure and behavior was shown through **PCL-3k** first, followed by the effect of incorporation into a conventional TPU in **BDO-PU**. The effect of DA bonds on TPU behavior was then evaluated through comparison with **DA-PU**, and substantial changes in thermal, morphological and rheological behavior were shown to occur upon each of these modifications.

■ MATERIALS AND METHODS

Materials

Poly(ε-caprolactone) polyol (Capa 2302AJ) (M_n = 3.1 kg mol^{-1}, $Đ$ = 1.5) (**PCL-3k**, Figure 1) was provided by Ingevity (Warrington, UK). 4,4′-methylenebis (phenyl isocyanate) (98%), furfuryl alcohol, and 1,4-butanediol (99%) were purchased from Sigma Aldrich (St. Louis, MO, United States). 2-hydroxyethyl maleimide (HEMI) was provided by Henkel Corporation (Düsseldorf, Germany). Anhydrous toluene was obtained using a Grubbs solvent purification system. Furfuryl alcohol was distilled until colorless before use, all other reagents were used as received.

Synthesis of Polyurethane-Containing Butanediol Chain Extender

The **BDO-PU** copolymer (Figure 1) was prepared via a two-step prepolymer method to control the molecular architecture, ensuring a HS length of no more than two MDI monomers was maintained (Scheme S1, see Supporting Information). Capa 2302AJ (**PCL-3k**) was melted in a 250 mL flange flask and stirred with a magnetic stirrer under vacuum to remove moisture. After stirring for 1 h, 30 mL anhydrous toluene was added followed by MDI (2 equiv compared to **PCL-3k**) while refluxing at 110 °C, 150 rpm, and the reaction mixture was stirred for a further 1 h to make an isocyanate (NCO) functionalized prepolymer. Statistically, using 2 equiv of MDI is expected to prepare a mixture of chain topologies, including polyol chains terminated with MDI as well as some longer chains where MDI acts as a chain extender. Successful incorporation of MDI was confirmed by ^{1}H NMR (Figure S2) by the absence of the triplet peak at 3.60 ppm, corresponding to the aliphatic **PCL-3k** protons neighboring the terminal OH groups (Figure S1). A slight excess of 1,4-butanediol was then added to the prepolymer melt (1.2 equiv of BDO hydroxyl groups per free isocyanate group) to target a PU molecular weight of approximately 25 kg mol^{-1}. There was a sudden increase in viscosity over the following 15 min indicating the expected increase of molecular weight, causing stirring to stop. Reaction completion was confirmed by Fourier Transform Infrared (FTIR) Spectroscopy from the absence of the N=C=O stretch at 2275 cm^{-1}, and the product was poured into a silicone tray and allowed to cool to ambient temperature.

Synthesis of Diels–Alder Polyurethane Prepolymers

The thermoreversible **DA-PU** copolymer (Figure 1) was also prepared via a two-step prepolymer method (Scheme S2).[17] **PCL-3k** was melted in a 250 mL flange flask and stirred with an overhead stirrer under

Downloaded from pubs.acs.org/macrobx/article-pdf/doi/10.1021/acs.macromol.6c01484/6895818/ma-2026-014843.pdf by guest on 04 November 2026

https://doi.org/10.1021/acs.macromol.6c01484
Macromolecules XXXX, XXX, XXX−XXX

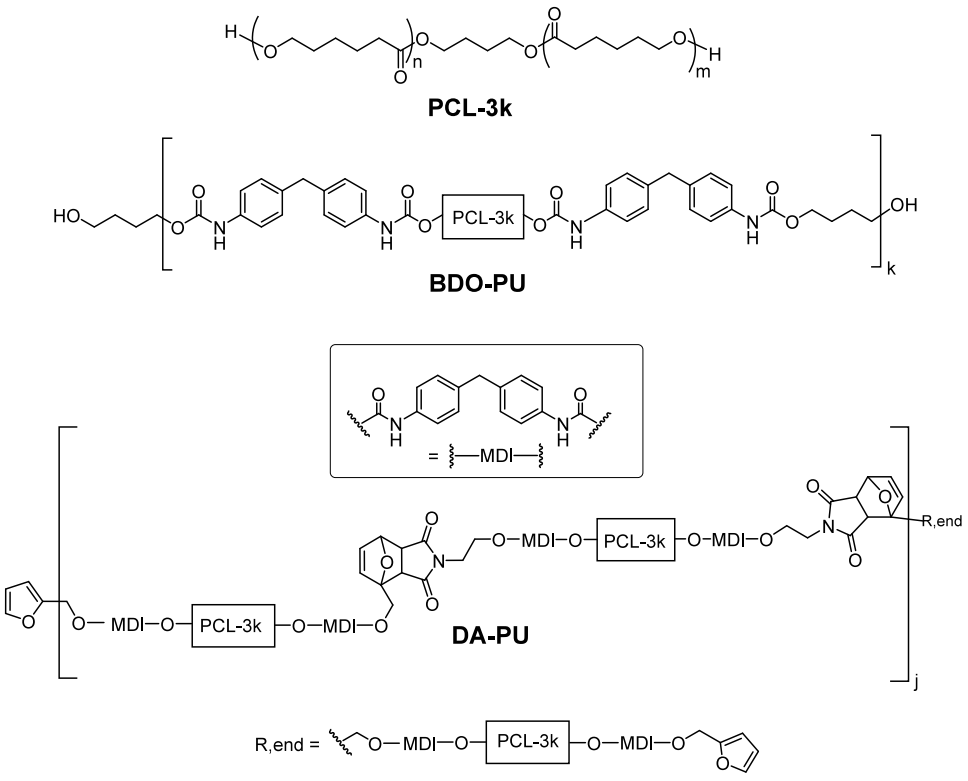


Figure 1. Chemical structures of **PCL-3k**, **BDO-PU** and **DA-PU**. The representative copolymer repeating units for **DA-PU** and **BDO-PU** are based on the 2:1 stoichiometry of MDI to **PCL-3k** in the first step of the reaction. In practice, only 2 equiv of MDI were used (compared to **PCL-3k**) so the product was a distribution of prepolymer chain lengths. Representative furan end groups are shown for **DA-PU** but the terminal groups can be furan or maleimide.

vacuum to remove moisture. After 1 h MDI was added (2 equiv compared to **PCL-3k**) while stirring at 110 °C, 150 rpm, and the reaction mixture was stirred for a further 1 h at 80 rpm to make NCO functionalized prepolymers. The chain ends were functionalized with furan or maleimide, by further reaction with furfuryl alcohol or HEMI, respectively (2.2 equiv compared to **PCL-3k**), while stirring at 110 °C, and the mixture was placed under a nitrogen atmosphere and allowed to react for a further 2 h. Reaction completion was confirmed by FTIR from the absence of the N=C=O stretch at 2275 cm^{-1}. In the case of the furfuryl prepolymer, excess furfuryl alcohol was then removed by vacuum distillation after this step. The prepolymer product was poured into a silicone tray and allowed to cool to ambient temperature.

Copolymerization of Diels–Alder Prepolymers to Prepare the Thermoreversible DA-PU Copolymer

After synthesis of the prepolymers, one molar equivalent of each **DA-PU** prepolymer with either maleimide or furan chain ends was weighed then cut up into small pieces, melted in a 250 mL flange flask at 110 °C and stirred with an overhead stirrer at 30 rpm for 15 min, then at 10 rpm for 10 min. The homogeneous melt was poured into a silicone tray and maintained at ambient temperature for one week to allow the formation of DA cycloadducts. SEC analysis revealed an increase in the molecular weight of **DA-PU** relative to the prepolymers (Table 1), confirming the successful progression of the DA reaction. Cycloadduct formation was also confirmed by ^{1}H NMR, where the low intensity peaks at approximately 5.3 and 6.5 ppm, corresponding to protons within the cycloadduct structure,[32] were observed (Figure S3).

Proton (^{1}H) Nuclear Magnetic Resonance. ^{1}H NMR spectra were recorded using a Bruker Avance 400 spectrometer 74 (400 MHz) using $CDCl_3$ as the solvent. All chemical shifts were recorded in parts per million (ppm) relative to a reference peak of chloroform solvent at $\delta = 7.26$ ppm.

Size Exclusion Chromatography (SEC). Measurements were performed using a 1260 Infinity instrument (Agilent, Santa Clara, CA, United States) with a refractive index detector. Two Agilent PL-gel 5 μm Mixed-C columns and a guard column were connected in series and maintained at 35 °C. HPLC grade chloroform containing 0.25% v/v NEt_3 was used as the eluent and the flow rate was set at 1.0 mL min^{-1}. The molecular weight calculation was performed on the Agilent software, against a calibration using a series of poly(methyl methacrylate) (PMMA) standards.

Differential Scanning Calorimetry (DSC). Measurements were performed using a Discovery DSC 25 (TA instruments, New Castle, DE, United States) on approximately 3 mg samples loaded into aluminum DSC pans (TA Instruments, Wilmslow, UK). The difference in heat flow between the sample and a reference material (an empty DSC pan) as a function of temperature was measured under a nitrogen atmosphere at a heating and cooling rate of 10 °C min^{-1}. DSC was also employed to determine the glass transition temperature (T_g) and the melting point (T_m). In addition, isothermal experiments were performed to determine the crystallization kinetics of the studied polymers over a range of temperatures. In these experiments, the samples were first heated at a rate of 10 °C min^{-1} to the selected annealing temperature (T_a), held at that temperature for 5 min, and then cooled at 60 °C min^{-1} to the chosen crystallization temperature (T_{ic}), where isothermal crystallization was maintained for at least 30 min.

Time-Resolved Simultaneous SAXS, Wide-Angle X-Ray Scattering (WAXS), and DSC Measurements. Measurements were carried out using a Xeuss 2.0 laboratory instrument (Xenocs, Grenoble, France) equipped with a GeniX 3D copper X-ray source (Xenocs, Grenoble, France) (wavelength of X-ray radiation $\lambda_X = 1.542$ Å)

Downloaded from pubs.acs.org/macrobx/article-pdf/doi/10.1021/acs.macromol.6c01484/6958018/ma-2026-014843.pdf by guest on 04 November 2026

https://doi.org/10.1021/acs.macromol.6c01484
Macromolecules XXXX, XXX, XXX–XXX

Table 1. Molecular Weight Data and Thermal Behavior of PCL-3K, BDO-PU, DA-PU, and the DA-PU Prepolymers

polymer	M_n (kg mol^{-1})[a]	M_w (kg mol^{-1})[b]	$Đ$[c]	T_g (°C)[d]	T_m(SS) (°C) (1st heat ramp)[e]	T_m(SS) (°C) (2nd heat ramp)[f]	ΔH_m (SS) (J g^{-1}) (2nd heat ramp)[g]
PCL-3k	3.13	4.67	1.49	−62	57	50	77.6
BDO-PU	32.9	76.0	2.31	−46	49	45	34.7
DA-PU	25.7	82.8	3.22	−44	48	45	51.1
DA-PU furan prepolymer	9.36	19.8	2.11	−35	50	45	53.7
DA-PU maleimide prepolymer	9.81	20.2	2.06	−45	49	45	53.1

[a]Number average molecular weight. [b]Weight average molecular weight. [c]Dispersity (M_w/M_n), all molecular weight values listed here were determined by SEC (chloroform & TEA eluent, PMMA standards). [d]Glass transition temperature. [e]Soft segment crystalline melting point from first heat ramp. [f]Soft segment crystalline melting point from second heat ramp. [g]Soft segment melt enthalpy from second heat ramp.

with FOX 3D single reflection multilayered mirror. Pilatus 1 M and Pilatus 100 K two-dimensional hybrid pixel detectors (Dectris, Barden-Daetwil, Switzerland) were used for recording SAXS and WAXS patterns, respectively. SAXS data were collected over the range of 0.005 Å^{-1} ≤ q ≤ 0.3 Å^{-1}, while WAXS data were acquired over the range of 1.19 Å^{-1} ≤ q ≤ 3.53 Å^{-1} (14.5° ≤ 2θ ≤ 44.3°). The length of the scattering vector, q, is defined as $q = \frac{4\pi \sin\theta}{\lambda_X}$, where θ is half the scattering angle. Two-dimensional scattering patterns were integrated to give one-dimensional profiles and calibrated to absolute intensity using the XSACT software package supplied with the instrument. Sample discs of approximately 0.5 mm in thickness were sandwiched between two windows of cleaved mica (approximately 25 μm in thickness) and enclosed within aluminum DSC pans with holes for X-ray beam propagation. The prepared assemblies were subsequently mounted in a DSC600 heating stage (Linkam, Tadworth, UK). Samples were heated at a rate of 0.75 °C min^{-1} while continuously taking scattering patterns at a rate of 1 frame per 3 min.

Fourier Transform Infrared Spectroscopy. Measurements were performed using a Nicolet is50 spectrometer (ThermoFisher, Massachusetts, USA) set in transmission mode equipped with a DTGS room temperature detector with a KBr window. The instrument was purged with nitrogen during the measurements. A thin layer of the sample was cast from $CHCl_3$ onto a NaCl window (Edmund Optics, New Jersey, USA), which was fastened in a brass sample holder and heated using a high temperature circulating oil bath (Lauda Proline P5, LAUDA DR. R. WOBSER GMBH & CO. KG, Lauda-Konigshofen, Germany).

Oscillatory Shear Rheology. Measurements were performed on a MCR502 rheometer (Anton Paar, Graz, Austria) using parallel plate geometry. A 25 mm parallel-plate geometry was used for most measurements, while a 50 mm cone-plate geometry (2° cone angle) was employed for frequency sweeps of **DA-PU** at temperatures above 100 °C. Amplitude sweeps were performed to select a strain value within the linear viscoelastic region (LVER) before carrying out frequency and temperature sweep measurements. For the rheology measurements the samples were moulded into discs (a diameter of 25 mm and a thickness of 1 mm) using a vacuum compression molding device (MeltPrep, Graz, Austria).

■ RESULTS AND DISCUSSION

The molecular architecture of **DA-PU** (Figure 1) comprises three main components: a polyol soft segment (PCL), a diisocyanate hard segment (MDI), and DA bond-forming groups (maleimide and furfuryl). Each component exhibits distinct thermal behavior, giving rise to different structural morphologies. PCL, a semicrystalline polymer, can crystallize within a specific temperature range to form periodic lamellar structures. MDI, forming urethane bonds, establishes hydrogen bonding at lower temperatures, reinforcing the material. Maleimide and furan groups form DA covalent bonds that dissociate at elevated temperatures. The overlap of these temperature-dependent processes should produce a complex thermal response and morphology in **DA-PU**. To characterize its structure systematically, the presented analysis proceeded in increasing order of architectural complexity: first, the PCL polyol in its homopolymer state (**PCL-3k**); second, a reference TPU (**BDO-PU**) comprising **PCL**, **MDI** and **BDO**; finally, the **DA-PU** also comprising **PCL** and **MDI** but containing **DA** bonds as cycloadducts (Table 1).

Molecular Weight Distributions of the PU Copolymers

The molecular weight distribution of **BDO-PU** was characterized by SEC (Figure 2A and Table 1). An M_n value of approximately 33 kg mol^{-1} was obtained indicating the copolymerization was successful. The obtained dispersity value of 2.3 is typical of polymers produced by step-growth polymerization taken to high conversion.[33] As the measurements were performed against PMMA calibrants, the M_n and M_w values obtained are not absolute but are used in this work as relative comparisons between like materials. The molecular weight distribution of fully associated (DA-bonded) **DA-PU** is comparable to that of **BDO-PU** (Figure 2A); however, a higher dispersity ($Đ = M_w/M_n$) was observed (Table 1). **DA-PU** is synthesized by separately preparing two prepolymers, which are then blended to form a homogeneous mixture, followed by copolymerization at ambient temperature. Upon cooling, the prepolymers begin to crystallize, and the reaction proceeds to the solid state. As a result, the limited mobility of the polymer chains during this stage is likely to lead to the formation of polymers with a relatively broad molecular weight distribution. Furthermore, the association of the two **DA-PU** prepolymers, which exhibit slightly different molecular weight distributions to each other (Table 1), is expected to yield a copolymer with a broader molecular weight distribution.

After conditioning the **DA-PU** samples at ambient temperature to ensure DA bond formation, samples of **DA-PU** were then held at different temperatures to evaluate the effect of temperature on DA bond dissociation. Each sample was then quickly dissolved in chloroform and measured by SEC at 35 °C (Figure 2B). Chloroform was chosen as the eluent because dissociated **DA-PU** samples showed no molecular-weight change after 24 h, confirming negligible cycloadduct reformation in this solvent. A slight change in molecular weight is observed at temperatures below 60 °C (Figure 2B). In contrast, annealing at temperatures above 60 °C leads to a substantial reduction in molecular weight, attributed to the fast progression of the retro Diels–Alder reaction. At temperatures exceeding 100 °C, M_w

Downloaded from pubs.acs.org/macrobx/article-pdf/doi/10.1021/acs.macromol.6c01484/6895018/ma-2026-014843.pdf by guest on 04 November 2026

https://doi.org/10.1021/acs.macromol.6c01484
Macromolecules XXXX, XXX, XXX–XXX

decreases monotonically, whereas M_n demonstrates some fluctuations before ultimately reaching approximately 10 kg mol^{-1} at 120 °C indicating complete dissociation of the **DA-PU** to the prepolymer level (Table 1).

Other thermally induced side reactions are known to take place in polyester polyurethanes, such as urethane bond dissociation and transesterification in the soft segment. The reduction in molecular weight observed (Figure 2B) is attributed to the rDA reaction due to the temperature range over which it takes place. Urethane dissociation has been observed above 150 °C, but generally takes place closer to 200 °C and so is unlikely to be a significant factor in this work.[34,35] Transesterification of PCL has been shown to take place at 160 °C within a few hours.[36] While the occurrence of these side reactions cannot be ruled out during long periods of annealing at elevated temperatures, previous work demonstrated good retention of mechanical properties in a near identical PCL- based DA TPU over several reprocessing cycles, suggesting any effect of side reactions on these materials is limited.[16] In addition, TGA analysis in that study showed good thermal stability well above 200 °C, while FTIR spectroscopy revealed no detectable changes in chemical composition following reprocessing. Irreversible homopolymerisation of maleimide groups has been reported in the literature upon heating crosslinked DA networks above 150 °C, leading to degradation through permanent crosslinking of the material.[37] However, no evidence of maleimide homopolymerisation was observed in the present work using any experimental techniques employed (DSC, FTIR and rheology), consistent with previous observations for DA TPUs.[16,17]

As an additional assessment of the thermal stability and reversibility of the DA bonds, one **DA-PU** sample was subjected to four consecutive heating-cooling cycles between ambient temperature and 200 °C at a heating rate of 10 °C min^{-1}. The sample was then allowed to equilibrate at ambient temperature for one week to enable reassociation of the DA bonds, after which a further DSC thermogram was recorded. The rDA enthalpy measured during the fifth and final heating cycle was very similar to that of the pristine sample (Figure S14), indicating that the capacity for DA cycloadduct formation was retained following repeated heating to 200 °C. Taken together, these results provide no evidence for significant irreversible side reactions involving the maleimide or furan groups under the heating conditions employed and suggest that **DA-PU** can withstand repeated heating to 200 °C at 10 °C min^{-1} without substantial loss of DA functionality.

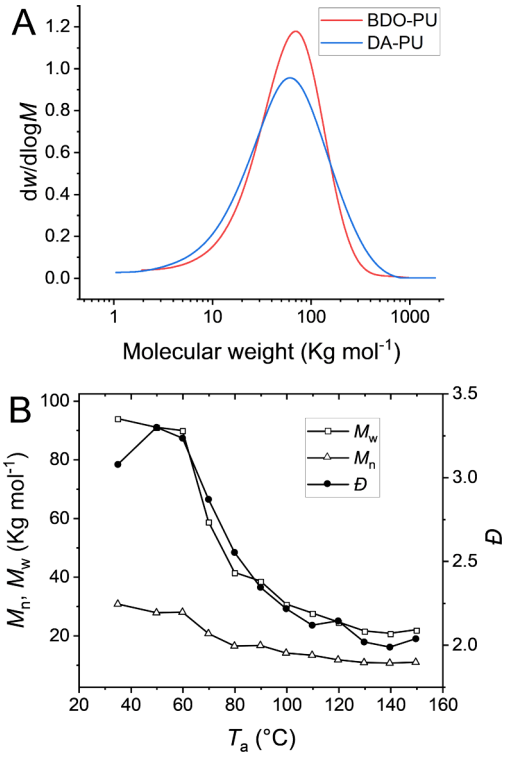


Figure 2. (A) Molecular weight distributions of **BDO-PU** and **DA-PU** measured by SEC. (B) Number and weight average molecular weight values as well as corresponding dispersity (M_n, M_w and $Đ$, respectively) for **DA-PU**, measured by SEC after annealing at different temperatures.

Thermal Properties

DSC was employed to investigate the effect of DA cycloadducts on the thermal behavior of the HS and SS of PU. In this respect, thermograms of polymers corresponding to SS only (**PCL-3k**), SS with HS (**BDO-PU**) and SS with HS and DA bonds (**DA-PU**) were compared with each other (Figure 3). The DSC data for **PCL-3k** were obtained from the second heating ramp after erasing the thermal history by heating the sample to 200 °C [well above the equilibrium melting point of poly(ε-caprolactone), T_m^0 = 64 °C],[38] and cooling it to –90 °C. A glass transition was observed at –62 °C (Figure 3), which is within the expected range for semicrystalline PCL.[39] A single endotherm was then observed at 50 °C, which is consistent with the melting of the PCL crystalline regions reported in the literature.[40]

The DSC thermogram of **BDO-PU** was likewise obtained after removal of the thermal history, using the same protocol applied to the **PCL-3k** sample. The glass transition was observed at –46 °C, representing a significant increase of 16 °C compared to **PCL-3k** (Figure 3). This suggests the occurrence of some phase mixing between the low T_g PCL soft segment and higher T_g BDO-MDI hard segment in **BDO-PU**,[41] resulting in an amorphous phase characterized by a higher T_g.

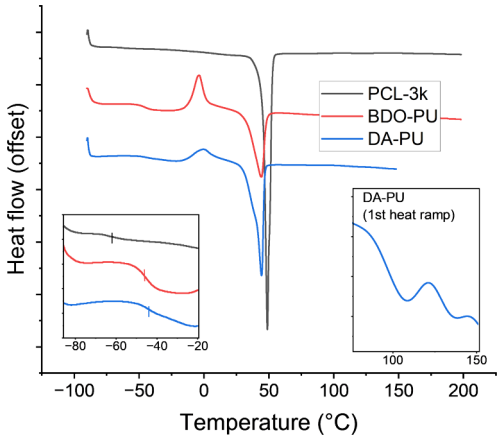


Figure 3. DSC thermograms of **PCL-3k** (black), **BDO-PU** (red) and **DA-PU** (blue) (endo down) recorded during the second heating ramp after removal of thermal history. The thermograms are vertically offset for clarity. The left inset highlights the glass transition regions of all materials. The right inset shows the endothermic transition region corresponding to the rDA reaction in **DA-PU**, as observed in the thermogram recorded during the first heating ramp.

Downloaded from pubs.acs.org/macromolbx/article-pdf/doi/10.1021/acs.macromol.6c01484/6895018/ma-2026-014843.pdf by guest on 04 November 2026

https://doi.org/10.1021/acs.macromol.6c01484
Macromolecules XXXX, XXX, XXX–XXX

During this second heating ramp, a cold crystallization exotherm was detected at 0 °C, followed by a melting endotherm at 45 °C, which can be attributed to the crystallization of the PCL soft segments upon release of chain mobility above T_g and their subsequent melting at elevated temperatures, respectively. The absence of cold crystallization in **PCL-3k** indicates that incorporation of hard segments in the PU architecture significantly alters SS (PCL) crystallization kinetics, degree of crystallinity, and melting behavior. The temperature of the SS melt endotherm in **BDO-PU** is depressed by approximately 5 °C in the second heat ramp in comparison to that of **PCL-3k**. When PCL oligomers are covalently bonded in a copolymer, PCL crystal growth along the chain direction stops when non-crystallizable MDI units are encountered. This reduces crystal size in the copolymer compared to the PCL homopolymer, lowering the polymer melting point. In addition, MDI units which are incorporated into SS crystals should act as defects, further reducing the melting point of the crystals.[42]

In analogy with the **BDO-PU** sample, the T_g of **DA-PU** (−44 °C) exceeded that of **PCL-3k** (−62 °C), indicating the formation of an amorphous mixed phase comprising of PCL soft segment regions with incorporated hard segment units. Furthermore, the marginally higher T_g of **DA-PU** relative to **BDO-PU** may indicate slightly enhanced miscibility of hard and soft segments, leading to a greater fraction of hard segment units dissolved within the amorphous phase and, consequently, elevated T_g although the difference is small. The cold crystallization and melt endotherm were also observed in the **DA-PU** thermogram at similar positions as in the **BDO-PU** thermogram, also pointing towards the suppressing effect of hard segment units on the PCL crystallization. In analogy with **BDO-PU**, no thermal transitions were detected in the **DA-PU** thermogram at temperatures above 50 °C during the second heating ramp. In contrast, the first heating ramp of **DA-PU** exhibited a double endothermic transition at 115 and 140 °C (Figure 3, right inset), corresponding to the rDA reaction temperatures (T_{rDA}) of the *endo* and *exo* diastereomers of the DA cycloadduct, respectively (Scheme 1).[43] These observations indicate that, once cleaved during the first heating cycle, the DA cycloadducts do not reform within the experimental time scale of the DSC measurement (about 1 h), resulting in the absence of the corresponding thermal signatures upon subsequent heating.

DSC results also show that **DA-PU** has a higher ΔH_m(SS) than **BDO-PU** (Figure 3 and Table 1) indicating a higher degree of SS crystallinity. This suggests that the SS in **DA-PU** crystallizes more easily than in **BDO-PU**, provided that it is crystallized from the melt at temperatures above T_{rDA}. This is likely a consequence of the lower molecular weight of **DA-PU** obtained after heating above T_{rDA}, enhancing the mobility of the copolymer chains and facilitating faster crystallization kinetics.

To examine the influence of the PU molecular architecture and the presence of DA cycloadducts on the crystallization kinetics of PCL in more detail, isothermal crystallization DSC experiments were performed over a range of temperatures (Figure 4). The DSC profiles collected were analyzed by the Avrami equation:[44]

$$1 - V_c(t) = \exp(-kt^n) \quad (1)$$

$$\log\left[-\ln(1 - V_c\ (t - t_0))\right] = \log(k) + n\log(t - t_0) \quad (2)$$

where V_c is the relative degree of crystallinity, k is the crystallisation rate constant, t is time, t_0 is the induction time (i.e., the time required for crystallisation to begin), and n is the Avrami exponent which reflects the combined contributions of nucleation and crystal growth mechanisms:

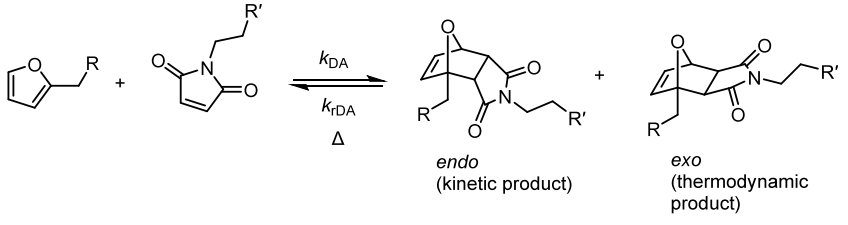
$$n = n_n + n_{gD} \quad (3)$$

where n_n is a value between 0 and 1 that describes the degree to which nucleation is instantaneous ($n_n = 0$) or sporadic ($n_n = 1$) and n_{gD} is an integer between 1 and 3 representing the dimensionality of crystal growth. The isothermal experiments and subsequent Avrami analyses (Figure 4 and Table 2) were performed according to guidelines by Lorenzo et al.[45]

Using eq 2, Avrami plots were constructed (e.g., for **PCL-3k**, Figure 4B) and a linear regression was fitted to the resulting straight lines corresponding to primary crystal growth (V_c is within the region of 0.03–0.2) to avoid crystalline impingement and ensure valid interpretation of the Avrami exponent. For **PCL-3k**, n values between 2.5 and 2.9 were obtained. Given that **PCL-3k** should have a spherulitic crystal morphology,[40] the obtained values are lower than the expected range between 3 and 4. However, similar n values have been reported in the literature for poly(ε-caprolactone)[40,46] and for other spherulitic aliphatic polyester homopolymers.[47] Despite the seemingly low n values, growth of **PCL-3k** spherulites with instantaneous nucleation is usually assumed.[48] An increase in n with crystallization temperature, T_{ic}, was observed for each material evaluated (Table 2). This is due to the increased occurrence of sporadic nucleation from greater thermal fluctuations.[49]

Slightly lower n values were obtained for **BDO-PU** compared to those of **PCL-3k** (Table 2), indicating that incorporation of PCL into the TPU copolymer alters the PCL crystallization mechanism. This observation suggests that the attachment of non-crystallizable segments to the PCL chains disrupts the regular molecular packing within the crystals, introducing directional growth. This disruption truncates the spherulite development and reduces the dimensional growth component n_{gD}.[42]

Scheme 1. Diels–Alder Cycloaddition of Maleimide and Furan



https://doi.org/10.1021/acs.macromol.6c01484
Macromolecules XXXX, XXX, XXX−XXX

Downloaded from pubs.acs.org/macromolbx/article-pdf/doi/10.1021/acs.macromol.6c01484/6895818/ma-2026-014843.pdf by guest on 04 November 2026

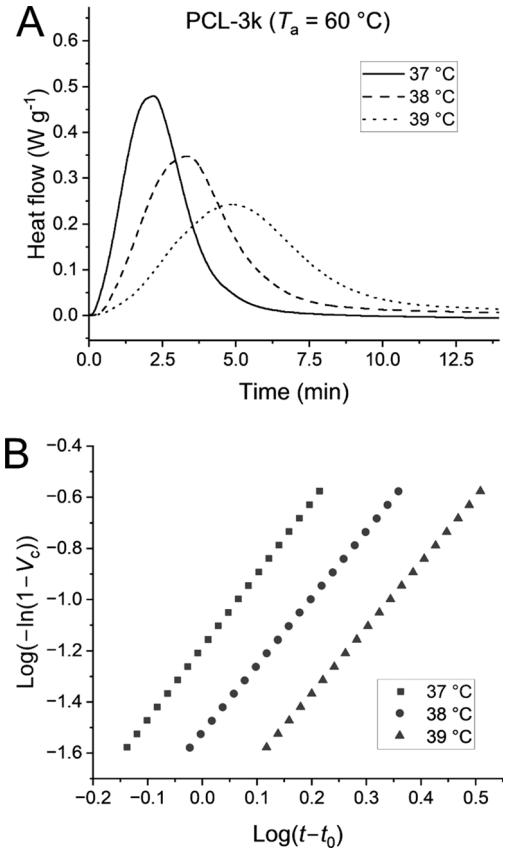


Figure 4. Representative heat flow curves recorded during isothermal crystallisation of **PCL-3k** at a range of T_{ic} (37–39 °C) after annealing at 60 °C (A) and corresponding Avrami plots (B).

Table 2. Isothermal Crystallisation Results for PCL-3k and the TPU Copolymers

sample	T_a, °C[a]	T_{ic}, °C[b]	n[c]
PCL-3k	60	37–39	2.55–2.84
DA-PU	60	8–20	2.09–2.26
DA-PU	150	22–32	1.99–2.14
BDO-PU	60	18–28	2.31–2.60
BDO-PU	150	18–28	2.38–2.51

[a]Annealing temperatures used in the experiment. [b]Crystallization temperatures used for isothermal crystallization. [c]Avrami exponent.

The crystallization half-time ($t_{1/2}$), determined as the time at which V_c reached 0.5, was taken to compare the crystallization kinetics of the materials (Figure 5). A different crystallization temperature range was chosen for each material to ensure that the crystallization was fully complete within a practical time period. The data for the **BDO-PU** were all displaced to lower temperatures compared to **PCL-3k**, showing that a greater degree of supercooling was required to crystallize the TPU copolymer soft segment. The increase in T_g observed for **BDO-PU** (Table 1) indicated that it has lower molecular mobility than **PCL-3k**, likely due to a combination of the higher molecular weight and the presence of interchain hydrogen bonding involving the HS urethane groups. All these factors should inhibit the PCL crystallization kinetics in **BDO-PU.**

The incorporation of DA bonds in the **DA-PU** copolymer in addition to the typical PU composition should add another level of complexity to the crystallization behavior of PCL. In this case the molecular weight of **DA-PU** changes dynamically depending on the applied temperature treatments (Figure 2B). This raises the question of how molecular weight affects the crystallization behavior at different thermal processing conditions. In this respect, isothermal crystallization DSC experiments were performed to investigate the crystallization behavior of the PCL soft segment in **DA-PU** using two different annealing temperatures: T_a = 60 °C (where $T_m < T_a < T_{rDA}$), and T_a = 150 °C ($T_m < T_{rDA} < T_a$).

The results for **DA-PU** show that the annealing temperature, T_a, has a significant impact on the crystallization kinetics (Figure 5). When annealed at 150 °C, **DA-PU** crystallized at significantly faster rates and at higher crystallization temperatures than when annealed at 60 °C. This difference is attributed to the temperature-dependent molecular architecture of **DA-PU**. At 150 °C, the rDA reaction promotes dissociation of the cycloadducts, resulting in a reduction in molecular weight and, consequently, increased molecular mobility. In contrast, annealing at 60 °C largely preserves the coupled architecture because the rDA reaction does not occur to a significant extent at this temperature. The molecular-weight state established during annealing is, therefore, an important factor governing the subsequent crystallization behavior, in addition to the thermal history itself.

During subsequent cooling, DA reassociation may occur; however, the kinetics of cycloadduct formation are slower than those of PCL crystallization. Consequently, a significant fraction of the molecular-weight reduction generated during annealing at 150 °C is expected to persist over the timescale relevant to crystallization, thereby facilitating soft-segment crystallization. This interpretation is further supported by the reference **BDO-PU**, for which the crystallization behavior remains similar after annealing at 60 and 150 °C (Figure 5), indicating that the pronounced dependence on T_a observed for **DA-PU** is associated with the reversible DA/rDA chemistry rather than thermal history alone. It should also be noted that the **DA-PU** crystallization after annealing at 60 °C was slower in comparison with the **BDO-PU** despite its similar molecular weight (Figure 2A). This **DA-PU** behavior at 60 °C could be related to the presence of DA units reducing molecular mobility of **DA-PU** in the high molecular weight state, as shown by its higher T_g (Table 1) and higher viscosity compared to **BDO-PU**. However, it may also be related to differences in molecular weight distribution of the materials (Figure 2A) as **DA-PU** shows a higher dispersity and M_w than **BDO-PU.**

Irrespective of T_a, The Avrami exponent obtained for **DA-PU** is lower than for **PCL-3k**, in analogy to the **BDO-PU** results (Table 2). While the crystallization rate of **DA-PU** showed a strong dependence on T_a, n was essentially unaffected. From this observation it can be inferred that annealing temperature, and thus **DA-PU** molecular weight, does not significantly affect the crystal growth dimensionality.

Overall, the isothermal crystallization results indicate that incorporation of DA bonds into the TPU does not significantly affect the dimensionality of SS crystal growth and thus does not significantly alter crystal morphology. On the contrary, the rate of crystallization was much higher in **DA-PU** compared to **BDO-PU**, but only after annealing at sufficiently high

Downloaded from pubs.acs.org/macmobx/article-pdf/doi/10.1021/acs.macromol.6c01484/6895018/ma-2026-014843.pdf by guest on 04 November 2026

https://doi.org/10.1021/acs.macromol.6c01484
Macromolecules XXXX, XXX, XXX–XXX

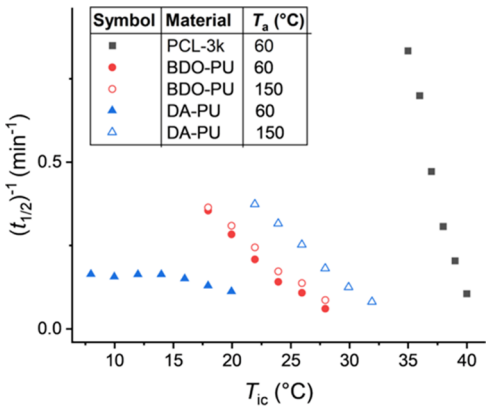


Figure 5. Effect of crystallisation temperature (T_{ic}) on the rate of crystallisation for **PCL-3k** and the TPU copolymers. The polymer name and the annealing temperature (T_a) are specified in the legend.

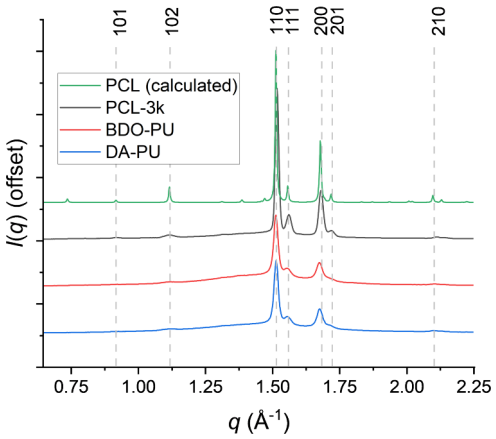


Figure 6. Experimental WAXS patterns of **PCL-3k** (black), **BDO-PU** (red), and **DA-PU** (blue), together with the calculated X-ray diffraction pattern of poly(ε-caprolactone) (green). The calculated pattern was generated using the reported crystal structure of poly(ε-caprolactone) corresponding to the orthorhombic $P2_12_12_1$ space group.[50] Miller indices are assigned to the calculated diffraction peaks based on this crystal structure. The patterns are vertically offset for clarity.

temperatures to break DA cycloadducts. This suggests the crystallization rate of **DA-PU** could be tuned via the annealing temperature.

Analysis of Structural Morphology

To obtain further insights into the effect of the DA bonds on the structural morphology of the TPUs, a comparative SAXS and WAXS analysis of **PCL-3k**, **BDO-PU** and **DA-PU** was performed. WAXS patterns of **PCL-3k** (Figure 6) exhibited diffraction peaks consistent with an orthorhombic unit cell having parameters $a = 7.46$ Å, $b = 4.97$ Å and $c = 17.06$ Å, in excellent agreement with the literature values of $a = 7.47$ Å, $b = 4.98$ Å and $c = 17.05$ Å reported for poly(ε-caprolactone) crystallizing in the orthorhombic $P2_12_12_1$ space group.[50] Moreover, the diffraction peak intensities were in good agreement with the calculated pattern using poly(ε-caprolactone) crystal structure data (Figure 6).[50,51] The high intensity 110 and 200 peaks are a very common feature associated with an all-trans 'zigzag' configuration of the polymer backbone crystallizing in an orthorhombic unit cell similar to the crystal structure of polyethylene.[52] The WAXS patterns of the TPU copolymers display a series of diffraction peaks similar to those of **PCL-3k**, indicating that the soft segments adopt the poly(ε-caprolactone) crystal structure in the solid state. Signs of appreciable hard segment crystallinity were not observed in either TPU material, possibly due to the short hard block length comprising only two MDI units.[53] The most noticeable change from **PCL-3k** to **BDO-PU** and **DA-PU** was the decrease in intensity of the poly(ε-caprolactone) diffraction peaks (Figure 6, see 110 and 200 peaks for the comparison), and conversely the increase in intensity of the amorphous halo, caused by a reduction in the total volume fraction of crystalline PCL component in the **TPU** materials compared to **PCL-3k**. Thus, the WAXS results confirm the reduction in PCL crystallinity within the TPUs, consistent with the DSC measurements [Table 1, see ΔH_m (SS)], and indicate that no change in the crystal phase structure of PCL occurred upon incorporation of the **PCL-3k** polyol into the TPU copolymers.

The polymer structure formed at larger (nanometer) scale was analyzed by SAXS. In particular, the evolution of structural morphology with temperature was followed via simultaneous time-resolved SAXS/WAXS/DSC measurements of **PCL-3k**, **BDO-PU** and **DA-PU**. The SAXS patterns of **PCL-3k** taken during heating from ambient conditions up to 40 °C showed a primary diffraction peak at $q^* = 0.052$ Å^{-1} accompanied by a second order peak at $q = 2q^*$, indicative of the presence of a lamellar morphology with the period of $L_p = 120$ Å ($=2\pi/q^*$) (Figure 7A). This structural morphology is typical of semicrystalline polymers such as **PCL-3k**, which forms through phase separation of amorphous and crystalline domains during polymer crystallization. Upon further heating to 54 °C, just below T_m measured by DSC during the first heating ramp (Table 1), the primary peak shifts towards the lower q values (L_p increases from 120 to 128 Å) and decreases in intensity. This shift is indicative of lamellar thickening, which occurs as thinner and less stable lamellae melt preferentially at elevated temperatures, leaving behind thicker lamellae containing larger and more thermally stable crystals. The concomitant decrease in peak intensity suggests a reduction in the overall degree of crystallinity and structural order as the system approaches melting state. Simultaneously, a new peak appears in the SAXS patterns at $q \sim 0.029$ Å^{-1} (Figure 7A), corresponding to a characteristic structural periodicity of about 213 Å. The position of this peak, close to $q = q^*/\sqrt{3}$, indicates that the **PCL-3k** transitions from its lamellar morphology and melts through a parahexagonal close-packed cylindrical morphology, as reported previously.[54,55] This structural transformation should be attributed to the low molecular weight of **PCL-3k**, which imparts high chain mobility and enables fast relaxation into alternative morphology under slow heating conditions. Heating above 54 °C results in a significant reduction in scattering intensity, followed by a featureless scattering pattern at temperatures above 56 °C (Figure 7A). At this point, the sample had melted, as confirmed by the melting peak observed in the DSC curve and the disappearance of the most intense 110 poly(ε-caprolactone) diffraction peak (Figure 7B).

The SAXS patterns of **BDO-PU** (Figure 7C), collected at the beginning of heating from ambient temperature, exhibited a broad scattering peak at $q = 0.043$ Å^{-1} which is likely to be related to a lamellar structural morphology with a periodicity of $L_p = 145$ Å. Upon heating, this peak broadened and shifted

Downloaded from pubs.acs.org/macrobx/article-pdf/doi/10.1021/acs.macromol.6c01484/6895018/ma-2026-014843.pdf by guest on 04 November 2026

https://doi.org/10.1021/acs.macromol.6c01484
Macromolecules XXXX, XXX, XXX–XXX

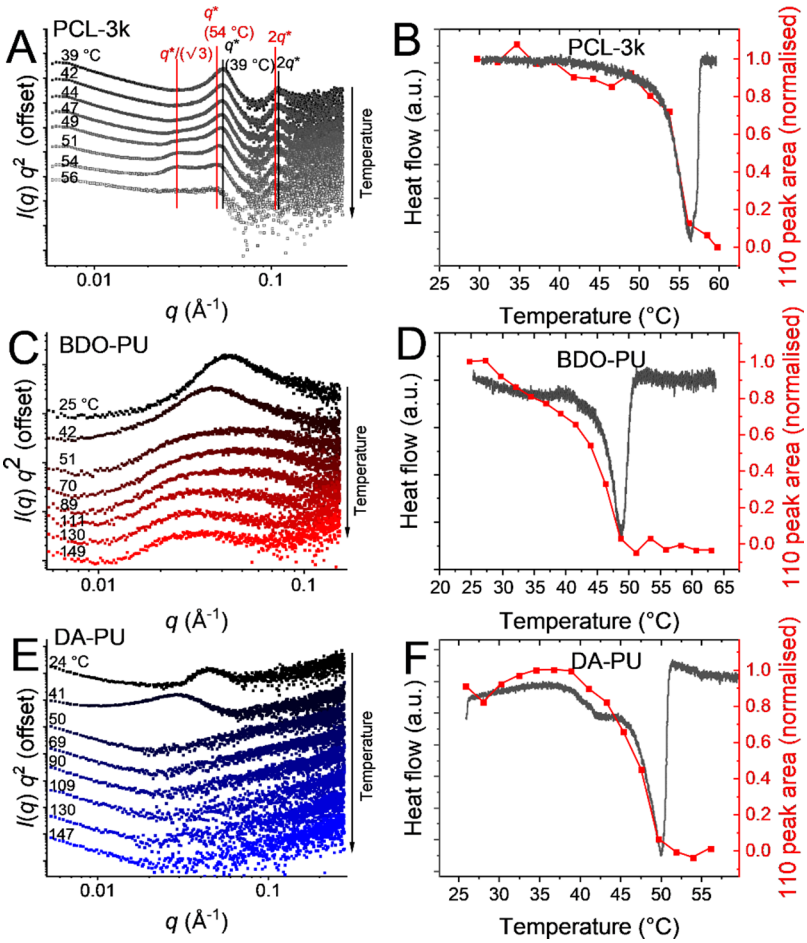


Figure 7. Simultaneous time-resolved SAXS (left column plots) and WAXS/DSC (right column plots) results for **PCL-3k**, **BDO-PU** and **DA-PU** (A and B, C and D, E and F, respectively) collected during a heating ramp (39–56 °C, 25–149 °C and 24–147 °C, respectively). SAXS patterns were Lorentz-corrected and offset by arbitrary values to avoid overlapping. The **PCL-3k** SAXS peaks are labelled at the initial temperature of 39 °C (black) and at an elevated temperature of 54 °C (red). For WAXS, the 110 diffraction peak area, normalised to its maximum intensity, was plotted as a function of temperature and superimposed on the corresponding DSC thermogram. DSC data are plotted endo down.

to lower q values, accompanied by the appearance of a melt endotherm in the DSC curve and a reduction in the intensity of the 110 poly(ε-caprolactone) WAXS diffraction peak (Figure 7D), similar to the behavior observed for **PCL-3k** (Figure 7A,B). These results indicate melting of the PCL crystals and disintegration of the semicrystalline lamellar morphology. The larger L_p observed for solidified **BDO-PU**, compared to the pure PCL polyol (**PCL-3k**), likely arises from an increased thickness of the amorphous regions, resulting from the incorporation of hard segment units into the polyol chain. After the complete melting of the soft segment crystalline component, a very broad diffuse scattering feature, spanning over a range of $q \sim 0.02$–0.05 Å^{-1} (corresponding to real-space length scales of around 100–300 Å), remained at elevated temperatures (Figure 7C). This feature, which is absent in the SAXS patterns of **PCL-3k** (Figure 7A), should be attributed to phase separation between hard and soft segment domain regions in the molten polyurethane. The correlation distance of this separation should be controlled by the PU block lengths.[27,56] Consequently, above the T_m of the soft segment crystalline phase, **BDO-PU** forms a structured melt. When **BDO-PU** was further heated between T_m and 150 °C, the intensity of the diffuse feature gradually decreased with temperature, although it remained detectable even at 150 °C (Figure 7C). This indicates that heating the material promotes a gradual phase mixing; however, a fully homogenised melt was still not achieved even at 150 °C, indicating persistent phase separation between HS and SS over the temperature range studied.

For **DA-PU**, the SAXS pattern recorded at ambient temperature shows a single scattering intensity peak corresponding to a long period of $L_p = 138$ Å (Figure 7E). By analogy with **PCL-3k** and **BDO-PU** polymers (Figure 7A,C), this feature is attributed to a lamellar morphology associated with PCL crystalline domains present in the material (Figure 6). As the temperature increased and the PCL crystals began to melt, according to WAXS and DSC (Figure 7F), the SAXS peak became more intense and shifted to lower q values until T_m was surpassed, beyond which a featureless SAXS pattern remained ($T >$ 50 °C, Figure 7E). Thus, unlike **BDO-PU**, SAXS measurements of **DA-PU** demonstrate that no PU phase separation occurs in this material upon heating above the PCL T_m. It appears that the association of hard segment units is disrupted in **DA-PU**, leading to a more homogeneous material compared to conventional butanediol polyurethanes. This is likely to be related to the bulky, kinked structure of the DA cycloadduct chain extender which can inhibit hydrogen bonding between MDI

Downloaded from pubs.acs.org/macmobx/article-pdf/doi/10.1021/acs.macromol.6c01484/6895018/ma-2026-014843.pdf by guest on 04 November 2026

https://doi.org/10.1021/acs.macromol.6c01484
Macromolecules XXXX, XXX, XXX–XXX

units compared to the linear butanediol molecule. However, the difference in molecular weight dispersity in **DA-PU** and **BDO-PU** (Table 1) may also influence the phase separation behavior, but studies on the effect of molecular weight distribution of the total copolymer chain on phase separation with constant length and dispersity of each block are lacking in the literature. In addition, differences in chain end group structure could also be relevant. In particular, **BDO-PU** molecules are terminated by OH groups, whereas **DA-PU** molecules have furfuryl or maleimide groups at the termini, and potential compatibilization effects from the **DA-PU** end groups cannot be completely ruled out without further investigation.[57] Finally, the thermal history of a polyurethane can also have an effect on its phase separated morphology and hard segment structure,[58,59] but it would be challenging to investigate in this study as **DA-PU** dissociates at high temperatures (Figure 2B) and thus behaves differently to **BDO-PU** under the same thermal conditions.

Analysis and comparison of the SEC, DSC, WAXS and SAXS results obtained for **PCL-3k**, **BDO-PU** and **DA-PU** can be rationalized using a unified structural model that highlights the influence of DA bonds on the morphological organization of the TPUs investigated (Figure 8). Both **BDO-PU** and **DA-PU** consist of a semicrystalline PCL SS matrix containing a certain fraction of HS units. Within the soft segments, phase separation between crystalline and amorphous PCL domains gives rise to a periodic lamellar structure, as evidenced by SAXS and WAXS. In **BDO-PU**, the hard segments are essentially linear, owing to chain extension of the MDI units by linear butanediol (Figure 1). This linear architecture promotes efficient packing and aggregation of the hard segments, leading to pronounced HS-SS phase separation in addition to the crystalline-amorphous segregation within the soft segments. In contrast, in **DA-PU** the MDI units are chain-extended by non-linear DA cycloadducts (Figure 1) imparting a non-linear, kinked geometry to the hard segments (Scheme 1 and Figure 8, **right**). This structural irregularity suppresses hard-segment aggregation, resulting in a more homogeneous dispersion of HS units within the soft-segment matrix and significantly reduced HS-SS phase separation, while the lamellar morphology associated with crystalline-amorphous SS separation is retained.

Analysis of Intermolecular Forces and Diels–Alder Dissociation Kinetics by FTIR

To investigate the influence of DA bonds on the evolution of hydrogen-bonding interactions, temperature-dependent transmission FTIR measurements were performed on the studied polymers during heating from the PCL soft segment melting temperature up to 150 °C. Previous FTIR studies on polyurethanes, particularly those containing polyether soft segments, have commonly tracked the evolution of the urethane carbonyl stretching bands as a function of temperature.[53,58,60] However, this was practically very difficult as this band was obscured significantly by the SS ester carbonyl band (see Figure S4 and associated text in the Supporting Information).

The N–H bands recorded in the region of 3200–3500 cm^{-1} were more informative with two prominent absorption bands observed at 3344 and 3441 cm^{-1} (Figure 9), corresponding to stretching vibrations of hydrogen-bonded and free N–H groups, respectively.[61,62] Although easier to analyze than the carbonyl peak region (Figure S4), the broad hydrogen-bonded N–H band is known to be composed of at least three different N–H stretching modes.[63] Thus, quantitative analysis of the free and hydrogen-bonded groups is not possible without detailed peak deconvolution.[62,64] Therefore, the data generated in this investigation were used for a qualitative evaluation only. FTIR spectra collected during heating of **BDO-PU** and **DA-PU** show (Figure 9) that the position of the hydrogen-bonded N–H band shifted to higher frequency, from 3345 cm^{-1} at 50 °C to 3357 cm^{-1} at 150 °C. Based on similar observations reported previously, this behavior can be attributed to weakening of the hydrogen bonds with increasing temperature.[64] It is also noticeable from the FTIR spectra that the hydrogen-bonded N–H band diminishes with temperature whereas the free N–H band at around 3441 cm^{-1} becomes more intense. This results from the thermal dissociation of hydrogen bonds between urethane groups. The free N–H band has a smaller extinction coefficient

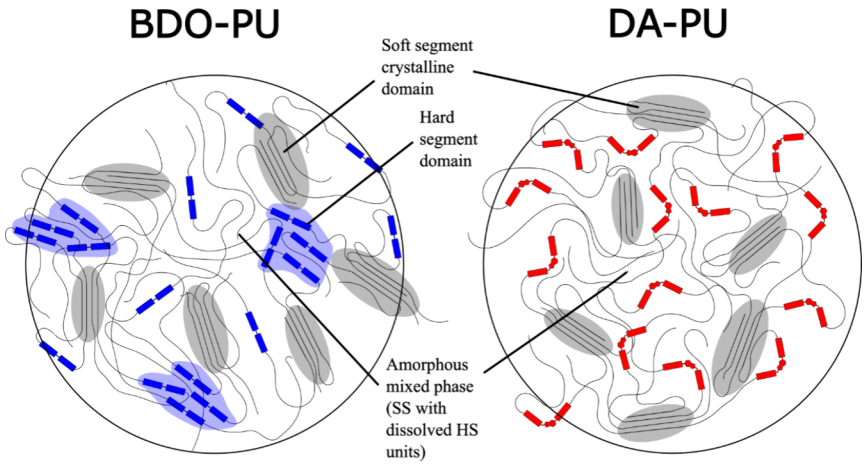


Figure 8. Schematic showing the proposed morphologies of **BDO-PU** (left) and **DA-PU** (right). The curved thin lines represent the amorphous PCL soft segment matrix, and the straight lines presented in stacks represent the crystalline soft segment lamellae. The blue/red rectangles represent the MDI groups in the hard segment of **BDO-PU** and **DA-PU**, respectively, and the line or polygon joining them represents the chain extender molecule. In **DA-PU**, the hard segments are kinked (non-linear) due to the shape of the DA cycloadduct.

Downloaded from pubs.acs.org/macromolbx/article-pdf/doi/10.1021/acs.macromol.6c01484/6895801/8/ma-2026-014843.pdf by guest on 04 November 2026

https://doi.org/10.1021/acs.macromol.6c01484
Macromolecules XXXX, XXX, XXX–XXX

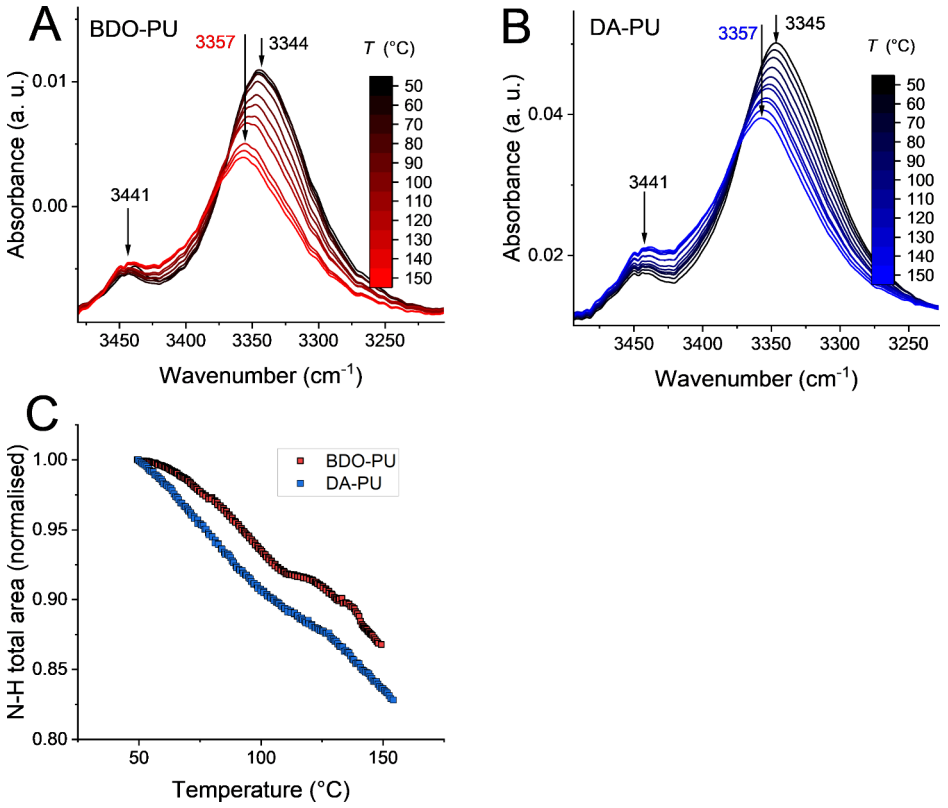


Figure 9. Evolution of N–H FTIR absorption bands with temperature in **BDO-PU** (A) and **DA-PU** (B), and temperature dependence of the total N-H band area calculated for **BDO-PU** and **DA-PU** (C).

and thus absorbs less strongly per concentration unit, meaning that the N–H region becomes less intense overall as the strength of the hydrogen bonding is reduced.[62] Thus, integrating the whole N–H region and plotting against temperature was used here to qualitatively show dissociation of hydrogen bonds with temperature without the need to identify and fit the peaks individually (Figure 9C).[61] Overall, the hydrogen bond dissociation behavior observed by FTIR appeared to be very similar for both **BDO-PU** and **DA-PU**, irrespective of their molecular architectures and associated morphological differences.

As much of the behavior of **DA-PU** is dependent on the relationship between the rDA reaction and temperature, it is essential to understand the kinetic and thermodynamic parameters that govern this relationship. FTIR spectroscopy can be employed for evaluating the dissociation of Diels–Alder cycloadducts. The free maleimide ring produces a band at 696 cm^{-1},[65,66] which increases in intensity as the DA cycloadducts dissociate into the constituent maleimide (M) and furan (F) units (Figure S5):

$$\mathrm{DA} \rightleftharpoons \mathrm{M} + \mathrm{F} \tag{4}$$

The area of this band was monitored while heating from 50 to 150 °C, and the temperature-dependent band area, $A(T)$, which is proportional to the concentration of free maleimide groups, was used to determine the fractional conversion of DA cycloadducts to free maleimide and furan for the rDA reaction $[w(T)]$:

$$w(T) = \frac{A(T)}{A(150\ ^\circ\mathrm{C})} \tag{5}$$

The temperature ramp plot obtained (Figure 10) shows that conversion begins to increase from 80 °C, rises sharply between 90 and 140 °C, and then starts to plateau around 150 °C. This plateau represents the onset of the thermodynamic limit of the rDA reaction, at which the majority of DA cycloadducts are dissociated.

FTIR time sweep experiments were performed with the aim to find the activation energy of the rDA reaction, which can be defined by the following elementary rate equation:[67]

$$\frac{d[\mathrm{M}]}{dt} = k_{\mathrm{rDA}}[\mathrm{DA}] - k_{\mathrm{DA}}[\mathrm{M}][\mathrm{F}] \tag{6}$$

where [M] is the concentration of free maleimide groups, t is time, k_{rDA} is the rDA reaction rate constant, [DA] is the DA cycloadduct concentration, k_{DA} is the rate constant of the DA cycloadduct formation reaction, and [F] is the concentration of free furan groups (which is approximately equal to [M]). The rate equation is more convenient to use with FTIR data when the concentration terms are replaced with the dimensionless conversion, x:

$$x(t) = \frac{A(t)}{A(150\ ^\circ\mathrm{C})} \tag{7}$$

Downloaded from pubs.acs.org/mamobx/article-pdf/doi/10.1021/acs.macromol.6c01484/6895018/ma-2026-014843.pdf by guest on 04 November 2026

https://doi.org/10.1021/acs.macromol.6c01484
Macromolecules XXXX, XXX, XXX–XXX

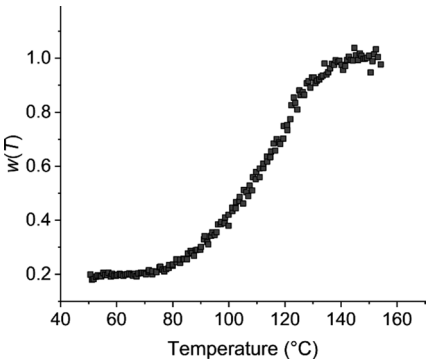


Figure 10. Retro Diels–Alder conversion $[w(T)]$ of **DA-PU** as a function of temperature, calculated from the free maleimide ring FTIR band area using eq 5. Obtained from a heat ramp at a constant heating rate of 1 °C min^{-1}.

where $A(t)$ is the area of the free maleimide peak at time t, and $A(150\ °C)$ is the maximum area of the maleimide peak reached after completion of the rDA reaction at 150 °C. Using eq 7 the maleimide band area can be converted into a conversion value between 0 and 1, corresponding to the fraction of remaining DA bonds in the material. Thus, eq 6 can be rewritten as:

$$\frac{dx}{dt} = k_{rDA}\cdot(1-x) - k_{DA}\cdot[M]_0\cdot x^2 \quad (8)$$

where $[M]_0$ is the total concentration of maleimide groups (free and in cycloadducts). If the forward reaction is observed, the negative form of eq 8 is taken:

$$-\frac{dx}{dt} = -k_{rDA}\cdot x + k_{DA}\cdot[M]_0\cdot(1-x)^2 \quad (9)$$

A more detailed derivation of eq 8 can be found in the Supporting Information eqs S1–S7. To characterize the kinetic and thermodynamic behavior of the DA bond dissociation in **DA-PU**, isothermal time sweep experiments were used to calculate the rDA reaction and DA association rate constants, k_{rDA} and k_{DA}, respectively. The experiments were performed over the range of 80–140 °C, where equilibrium progressively shifts towards the rDA reaction. The pre-equilibrated sample was placed in the FTIR spectrometer at ambient temperature and rapidly heated to the annealing temperature T_a, where it was held and measured by taking spectra until the area of the maleimide band at 696 cm^{-1} became constant. Using eq 8 to fit the obtained data (Figure 11A), the rate constants k_{rDA} and k_{DA} were extracted from the isothermal conversion curves. The activation energy of the rDA reaction (E_a) was then found from the Arrhenius plot (Figure 11B) using the universal gas constant (R = 8.31 J mol^{-1} K). An activation energy of 91.7 ± 5.02 kJ mol^{-1} determined for the rDA reaction is in good agreement with previously reported activation energies in the range of 90–100 kJ mol^{-1} for other DA systems utilizing furan and maleimide groups.[9,67–69] An activation energy could not be obtained for the forward DA reaction due to a lack of correlation between the k_{DA} parameter and T. It was noted that k_{DA} could be varied substantially without a significant reduction in the quality of the fit of the data (Figure S6), indicating that the performed measurements were not sufficiently sensitive to

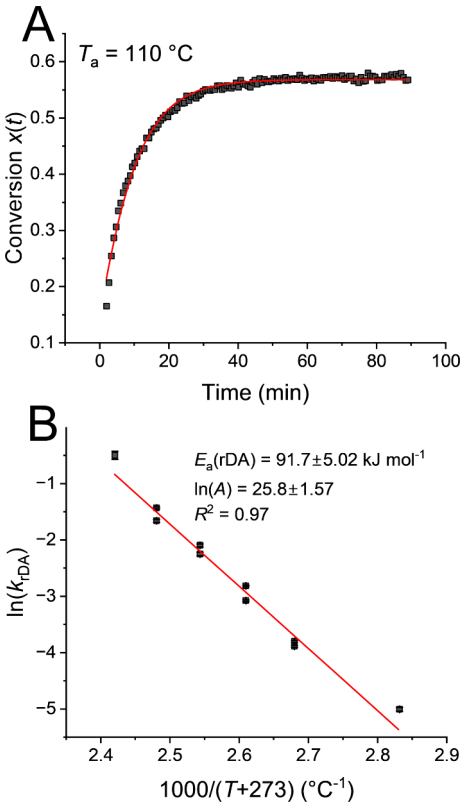


Figure 11. Representative isothermal conversion vs time curve for **DA-PU** at T_a = 110 °C (A). Arrhenius plot from k_{rDA} rate constant (B). Error bars are shown for ln(k_{rDA}) but are smaller than the data points.

allow reliable determination of k_{DA}. Performing experiments at lower temperatures and fitting the forward reaction with eq 9 would likely yield more meaningful values for k_{DA}, as the equilibrium is shifted towards the DA association reaction under these conditions, resulting in significantly larger k_{DA} values.

Viscoelastic Properties of TPUs

The difference in behavior observed between **DA-PU** and **BDO-PU** with respect to structural morphology (Figure 7) and dynamic molecular weight (Figure 2B) should influence rheological behavior. Thus, oscillatory shear rheology experiments were performed to investigate the viscoelastic properties of the polyurethanes studied. Firstly, temperature sweep measurements were performed on **BDO-PU** and **DA-PU** at a fixed angular frequency of 1 rad s^{-1} (Figure 12) at temperatures above their crystalline soft segment (PCL) melting points. There was a gradual decrease in **BDO-PU** complex viscosity (η^*) with an increase of temperature (Figure 12A). The storage and loss moduli data (G' and G'', respectively) of **BDO-PU** (Figure 12B) show solid-like behavior ($G' > G''$) up to approximately 90 °C, at which point a crossover ($G' = G''$) is observed. This rheological response indicates the presence of an entangled or physical network at low temperatures, which could arise from phase separation between HS and SS (Figure 8). Indeed, upon heating, a steep decline in G' takes place at temperatures between 70 and 120 °C. Consistent with this observation, SAXS results (Figure 7C) show that the primary broad

Downloaded from pubs.acs.org/macrobx/article-pdf/doi/10.1021/acs.macromol.6c01484/6895018/ma-2026-014843.pdf by guest on 04 November 2026

https://doi.org/10.1021/acs.macromol.6c01484
Macromolecules XXXX, XXX, XXX–XXX

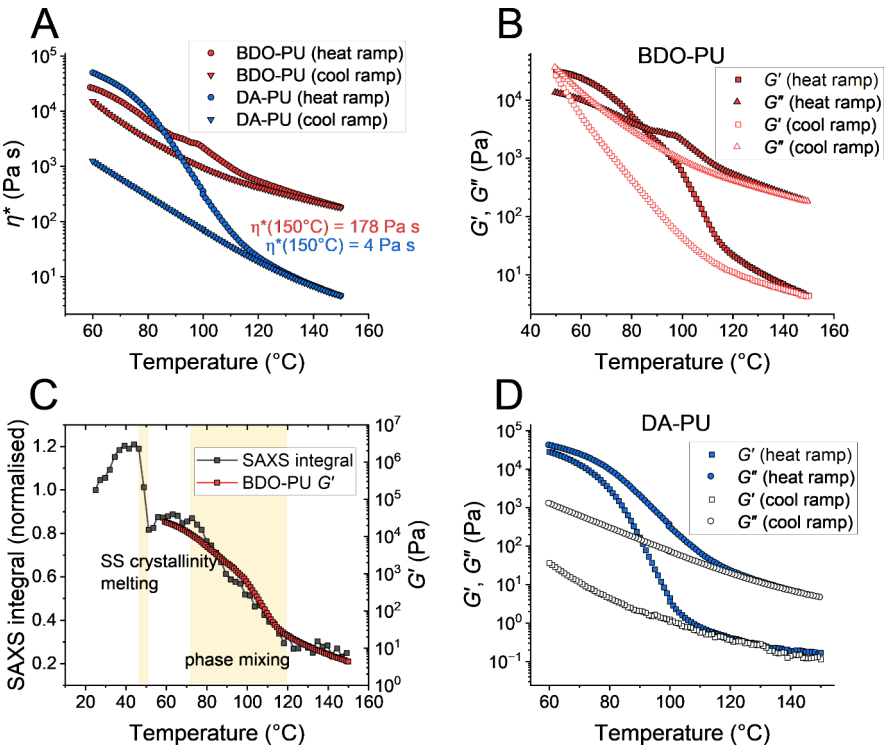


Figure 12. (A) Temperature ramp data of **BDO-PU** and **DA-PU** over the temperature range of 60–150 °C plotted as complex viscosity (η^*), (B) storage modulus G' and loss modulus G'' of **BDO-PU** plotted against temperature, (C) superimposed temperature dependence of G' and the area of the SAXS pattern of **BDO-PU** during heating (Figure 7C). (D) G' and G'' of **DA-PU** plotted against temperature. All rheological measurements were performed during temperature sweeps using a heating rate of 0.5 °C min^{-1}, cooling rate of 1 °C min^{-1}, and angular frequency ω of 1 rad s^{-1}. Strain amplitudes used were γ = 1% (**BDO-PU**) and γ = 1–10% linear ramp at T < 100 °C and 10% at $T \geq$ 100 °C (**DA-PU**).

peak associated with the PU phase separation progressively diminishes over the same temperature range. This correspondence suggests that the reduction in G' is driven by partial mixing of the hard and soft segments disrupting the phase-separated morphology. A similar rheological feature has previously been observed at temperatures just above the glass transition temperature of the HS, although no distinct hard-segment T_g was detected by DSC for **BDO-PU** (Figure 3). Nevertheless, a strong correlation was observed between the temperature dependence of G' and the normalized area of the SAXS pattern of **BDO-PU** at temperatures above the SS melting point (Figure 12C). This agreement further supports the direct link between the evolution of PU microphase separation and the macroscopic rheological behavior, in line with the literature report.[56]

In contrast, **DA-PU** exhibited liquid-like behavior ($G'' > G'$) from the very beginning of the heating temperature sweep (Figure 12D) in striking contrast to **BDO-PU** (Figure 12B). This observation indicates the absence of a strong physical network arising from phase-separated polyurethane hard- and soft-segment domains. This interpretation is further supported by the earlier SAXS results for **DA-PU** (Figure 7E) and is consistent with the proposed morphological model (Figure 8). For **DA-PU**, a sharp decrease in G', G'' and η^* is observed upon heating at temperatures above 80 °C (Figure 12A,D), consistent with the rDA dissociation indicated by FTIR (Figure 10). These rheological parameters plateau at approximately 120 °C, suggesting completion of the bond breaking rDA reaction, again in good agreement with the FTIR data. At 150 °C, **DA-PU** exhibits a melt viscosity of approximately 4 Pa.s (Figure 12A), consistent with thermal dissociation and reduction of molecular weight into prepolymers (Figures 2B and 10). In contrast, **BDO-PU**, which has a molecular weight comparable to that of **DA-PU** in its associated state (Figure 2A), displays η^* at 150 °C that is nearly 50 times higher (178 Pa s, Figure 12A). The combined effects of the phase-separated hard-soft segment morphology of **BDO-PU** (Figures 7C and 8) and its invariant molecular weight produce this pronounced difference in rheological properties. During the cooling ramp, **DA-PU** exhibited significantly lower η^*, G' and G'' values compared to the heating ramp (Figure 12D), reflecting the reduction in molecular weight caused by rDA dissociation. The reformation of DA cycloadducts is kinetically slow and occurs on a much longer timescale than that of the experiment. This prevents full recovery of the DA bonds during this cooling process.

BDO-PU exhibited conventional rheological behavior when analyzed by frequency sweeps at individual temperatures (Figure S7). At low temperatures, a rubbery plateau is observed with $G' > G''$ and a power-law dependence of $G' \propto \omega^{0.5}$. This behavior persists up to approximately 80 °C, where G' and G'' become equal, indicating the onset of the transition-to-flow region (gel point). At 100 °C, **BDO-PU** displays terminal flow behavior with $G'' >> G'$. The terminal power-law exponents of G' and G'' (1.6 and 1.0, respectively) deviate significantly from Rouse model predictions. Such deviations have previously been attributed to enhanced friction at the sharp interfaces between HS and SS domains.[70] Attempts to superimpose the **BDO-PU** rheological curves to construct a TTS master curve were

Downloaded from pubs.acs.org/macmobx/article-pdf/doi/10.1021/acs.macromol.6c01484/6895801 8/ma-2026-014843.pdf by guest on 04 November 2026

https://doi.org/10.1021/acs.macromol.6c01484
Macromolecules XXXX, XXX, XXX–XXX

unsuccessful (Figure S7). This failure indicates the presence of significant temperature-induced morphological changes. Consistent with this observation, the Han plot of **BDO-PU** (Figure S9A) shows a pronounced temperature dependence rather than a temperature-independent linear relationship between G' and G'' in double-logarithmic coordinates expected for homogeneous systems.[71] These rheological findings are in good agreement with SAXS results (Figure 7C), which reveal persistent hard-soft segment phase separation and a continuous evolution of the structural morphology across the studied temperature range.

While TTS fails for the **BDO-PU** rheological data (Figure S7), the **DA-PU** master curve (Figure S8) and Han plot (Figure S9B) exhibit much better coherence, despite the **DA-PU** dissociation occurring within the used experimental temperature window. In addition, the viscosity master curve obtained for **DA-PU** produced reasonable shear thinning and relaxation time parameters (see Figure S8B and the relevant discussion in the Supporting Information) comparable to a conventional TPU from the literature (Figure S10) which was measured at sufficiently high temperatures for hard-soft segment phase mixing to occur. This successful construction of a TTS master curve suggests that the **DA-PU** melt phase is more phase mixed than that of **BDO-PU**,[72,73] corroborating the proposed structural model (Figure 8) based on the conclusions drawn from the SAXS data. Despite the strong correlation between the horizontal shift factor and temperature (Figure S8C), suggesting that TTS can be suitable for predicting temperature-dependent viscoelastic behavior of **DA-PU**, the activation energy of flow ($E_{a,flow}$) calculated from the Arrhenius equation, eq S10, (193 kJ mol^{-1}, Figure S8C) is very high compared to that of ε-PCL homopolymer at $T_r > T_g +$ 100 K, which is around 35 kJ mol^{-1}.[74] This fact can be attributed to the thermal dissociation of **DA-PU**, which leads to a reduction in molecular weight and, consequently, a steeper temperature dependence of the material's viscoelastic properties.

The observed Arrhenius-type relationship between the horizontal shift factor and temperature (Figure S8C) suggests the superposition of two processes, both of which follow an Arrhenius relationship:

$$a_T' = a_T \cdot a_M \tag{10}$$

where a_T' is the observed temperature shift factor, a_T is the 'true' temperature shift factor, and a_M is a shift factor representing the contribution of the change in molecular weight. To isolate a_T in eq 10 a TTS master curve was constructed for the low molecular weight form of **DA-PU** by annealing at 150 °C before performing frequency sweep measurements at each individual temperature to ensure that most of the DA bonds were in the dissociated state during the measurements (Figure S11). The resulting 'true' $E_{a,flow}$ from the Arrhenius equation, eq S10, was 50.7 kJ mol^{-1} (Figure S11C), much closer to that of ε-PCL.[74]

In order to analyze the effect of molecular weight on **DA-PU** rheology, the same principle underlying the construction of the TTS master curve can be applied. A decrease in molecular weight linked to a decrease in the length of macromolecular chains gives them more mobility as would an increase in temperature.[75] In other words, the shape of the material's viscoelastic spectrum is universal with respect to changes in molecular weight as it is to changes in temperature, and there is a predictable relationship between the molecular weight of an entangled polymer and the position of its viscoelastic curve.[76] Theoretical justification of this principle was previously demonstrated by using reduced viscosity plots of η/η_0 against $\dot{\gamma}\eta_0$,[77] which was also supported by experimental evidence.[78] Han plots of a series of polymers with different molecular weights and narrow molecular weight distributions have been shown to overlap completely, provided that the molecular weight is significantly larger than the molecular weight between polymer entanglements, M_e.[79] From this, it was concluded that universal viscoelastic behavior is only observed when the system is fully dominated by entanglement effects. In further work on a series of polypropylene samples and a series of polyethylene-polypropylene copolymers of varying molecular weight time-molecular weight superposition (TMWS) master curves were successfully constructed.[75] It was demonstrated that the logarithms of the horizontal and vertical molecular weight shift factors (a_M and b_M) for the viscosity master curve exhibited a linear dependence on M_w. As previous works have demonstrated a valid basis for constructing a TMWS master curve, it provides a simple and convenient way of investigating the relationship between molecular weight and rheological properties of **DA-PU**, using a single sample to represent the full range of molecular weights.

To investigate the isolated effect of molecular weight on **DA-PU** rheology without the influence of changes in temperature, a **DA-PU** sample was measured at various molecular weights by subjecting it to a thermal cycle. This was achieved by heating the material and annealing it at a fixed temperature until equilibrium DA bond concentration and molecular weight were reached. The sample was then cooled to the reference temperature of 80 °C before performing a frequency sweep. The molecular weight distribution after each annealing step was known due to the SEC experiment (Figure 2B). As the time scale of the DA association reaction is slow compared to the time scale of the frequency sweep measurement, any reassociation of DA bonds occurring during the measurement was assumed to be negligible. The data obtained for each molecular weight (M) were then shifted to a reference molecular weight (M_r), constructing a TMWS master curve for **DA-PU** (Figure 13A,B). This was carried out using a similar procedure to the construction of the TTS, using horizontal (a_M) and vertical (b_M) molecular weight shift factors:

$$\omega(M_r) = a_M \cdot \omega(M) \tag{11}$$

$$G(M_r) = b_M \cdot G(M) \tag{12}$$

The obtained rheological results collapse well onto a master curve; however, noticeable differences are observed in terminal G' gradient at very low $a_M\omega$, which appears to increase as M_w decreases. The Han plot of the TMWS master curve also shows some disagreement (Figure S9C), but unlike the Han plot of the TTS (Figure S9B) the gradient remains mostly constant. This is likely because the TMWS was constructed using data collected only between 80 and 150 °C, where the change in molecular weight dispersity is less significant ($Đ$ = 2.6–2.0) compared with the broader molecular weight range used for the TTS analysis (T_a = 60–120 °C, $Đ$ = 3.2–2.1). While the change in gradient was minor, the vertical offset of the data sets was clear, caused by the steep vertical shift of the frequency

Downloaded from pubs.acs.org/macromolecules/article-pdf/doi/10.1021/acs.macromol.6c01484/6895018/ma-2026-014843.pdf by guest on 04 November 2026

https://doi.org/10.1021/acs.macromol.6c01484
Macromolecules XXXX, XXX, XXX–XXX

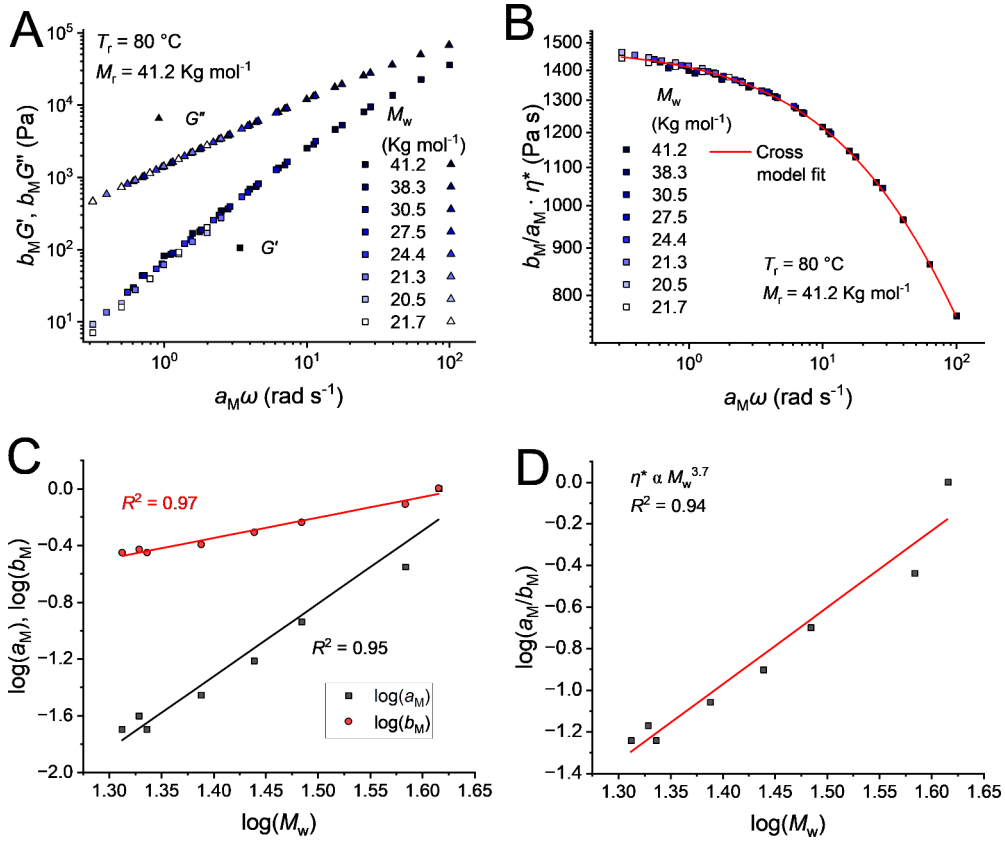


Figure 13. Time-molecular weight superposition master curve for **DA-PU** (T_r = 80 °C, M_r = 41.2 Kg mol^{-1}) plotted as moduli against angular frequency (A) and complex viscosity with Cross model fit, eq S12, (solid red line) against angular frequency (B). Common logarithm of horizontal (a_M) and vertical (b_M) molecular weight shift factors plotted against common logarithm of weight average molcular weight [log(M_w)] (C). Power law relationship between logarithm of complex viscosity and log(M_w) shown by a plot of log(a_M/b_M) against log(M_w) (D).

sweep data (Figure 13C). A linear relationship ($R^2 > 0.95$) was observed between the logarithm of the shift factors plotted against log(M_w) (Figure 13C), which validates the application of this procedure.

Since the equilibrium molecular weight of **DA-PU** is dependent on the temperature (Figure 2B), the plot of log(a_M) against log(M_w) can be converted to a plot of log(a_M) against T. This allows the influence of molecular weight on the activation energy of flow to be subtracted from the observed Arrhenius relationship using eq 10. By doing this, E_a was reduced from 193 to 73.4 kJ mol^{-1} (Figure S12), which was slightly higher than the value of 50.7 kJ mol^{-1} found from TTS of dissociated **DA-PU** in the low molecular weight form (Figure S11C). This suggests that the simple relationship proposed for the horizontal shift factor in eq 10 should be treated as a first approximation, and that additional factors should be considered to more accurately describe the temperature dependence of a'_T in **DA-PU.**

Inspection of the vertical shift factor plot shows a linear gradient between log(b_M) and log(M_w) (Figure 13C) with a minimum value of 0.35 reached by b_M at M_w = 23.9 kg mol^{-1}. According to the tube model for entangled polymers,[80] a change in molecular weight should theoretically have a significant effect on the horizontal shift factor a_M and b_M is expected to remain close to unity. This is because for an entangled polymer network the vertical position of the curve is mainly defined by the plateau modulus G^0_N, which in turn depends on the molecular weight between entanglements:

$$G^0_N = \frac{K\rho R\cdot(T+273)}{M_e} \tag{13}$$

where K is a constant (usually with a value of 4/5 for linear polymers),[81] ρ is the polymer mass density, T + 273 is the temperature in °C converted to the absolute temperature scale (K), and M_e is the molecular weight between entanglements dependent on the molecular architecture of the polymer and independent of its overall molecular weight. Since T was kept the same for the performed rheological measurements and changes in ρ with molecular weight are expected to be minor, no significant change in G^0_N should be expected. Despite this, b_M was shown to decrease with M_w (Figure 13C), indicating that G^0_N had an inverse relationship with molecular weight. This behavior may arise from the maleimide and furan end group concentration, which increases as molecular weight decreases, affecting the mechanical properties of the melt.

The dependence of viscosity on average molecular weight was determined by plotting log(a_M/b_M) against log(M_w) (Figure 13D), as this was more convenient than extrapolating to find zero-shear viscosity at each molecular weight. A power law relationship of $\eta^*_0 \propto M_w^{3.7}$ was observed, which is in reasonable agreement with the exponent of 3.4 expected for melts of monodisperse linear entangled polymers.[76] However, this value of 3.4 is based on systems where the vertical shift factor b_M is close to unity, and changes in viscosity are mainly

https://doi.org/10.1021/acs.macromol.6c01484
Macromolecules XXXX, XXX, XXX−XXX

Downloaded from pubs.acs.org/mamobx/article-pdf/doi/10.1021/acs.macromol.6c01484/6895818/ma-2026-014843.pdf by guest on 04 November 2026

associated with a_M. Taking the gradient of $\log(a_M)$ against $\log(M_w)$ for **DA-PU** gives a much larger value of 5.1, which agrees well with experimental results for the η_0 vs M_w relationship of other phase-mixed block copolymers.[82] This stronger dependence on M_w was attributed to differences in molecular friction coefficients between the two blocks. In this work, however, the decrease in entanglement modulus G_e with molecular weight effectively counteracts this effect for **DA-PU**, resulting in the observed relationship $\eta^*_0 \propto M_w^{3.7}$.

The TMWS viscosity master curve (Figure 13B) fitted using the Cross model, eq S12, produced similar parameters (η^*_0 = 1482 Pa s, $\lambda = 9.23 \times 10^{-3}$ and $m = 0.63$) in comparison with the TTS viscosity master curve (see Figure S8B and the relevant discussion in the Supporting Information). This shows that the shape and position of the master curve do not virtually change whether it is constructed via TTS or TMWS. The performed TWMS analysis enables the relationship between the rheological properties and molecular weight of **DA-PU** to be established. As the viscosity at each molecular weight, $\eta^*(M)$, can be calculated by multiplying that of the reference molecular weight, $\eta^*(M_r)$, by a_M/b_M:

$$\eta^*(M) = \frac{\sqrt{\left[\frac{1}{b_M}\cdot G'(M_r)\right]^2 + \left[\frac{1}{b_M}\cdot G''(M_r)\right]^2}}{\frac{1}{a_M}\cdot\omega} \tag{14}$$

$$\eta^*(M) = \frac{a_M}{b_M}\cdot\eta^*(M_r) \tag{15}$$

where the reference molecular weight (M_r) was taken as that of the sample with $M_n = 16.2$, $M_w = 41.2$ kg mol^{-1}, obtained after annealing at $T_a = 80$ °C. Assuming the molecular weight dependence of η^*_0 is the same as η^* from the TMWS master curves, plotting $\log(a_M/b_M)$ against $\log(M_n)$ allowed an empirical relationship to be established between η^*_0 and M_n (Figure S13):

$$\eta^*_0 \approx K\cdot M_n^{4.1} \tag{16}$$

where K is a temperature dependent constant. This relationship holds at higher states of dissociation (after annealing at $T_a \geq 90$ °C) where changes to dispersity were less significant (Figure 2B). As the concentration of DA bonds is directly proportional to M_n, the relative concentration of DA bonds in the material could be estimated as a function of time by the inverse of eq 16. As a result, the rate constant of the DA and rDA reactions can be determined from isothermal rheological measurements, enabling the activation energies of these reactions to be evaluated rheologically. While the activation energy of dynamic bond exchange in associative CANs (vitrimers) has commonly been elucidated through rheology via stress-relaxation measurements, this is not practical for a molten TPU.[83,84] Measuring E_a via the reaction conversion directly from the melt viscosity is more useful in this case, and a similar approach has been applied previously to characterize kinetics of PU bond dissociation.[34] Each experiment was performed in one of two ways depending on the measuring (annealing) temperature (T_a). For the high temperature measurements ($T_a \geq 90$ °C) a fully associated sample was loaded at 60 °C, then heated up to T_a, and the dissociation process (rDA reaction) was monitored by measuring η^*. For the low temperature measurements ($T_a < 90$ °C), a sample was loaded at 150 °C, allowed to dissociate fully, then rapidly cooled to T_a in order to monitor the DA bond reassociation (forward DA reaction) in the sample. From both experiments the fractional conversion (α) was estimated from plots of complex viscosity against time:

$$\alpha(t) = \frac{\eta^*(t)^{\frac{1}{4.1}} - \eta^*(t=0)^{\frac{1}{4.1}}}{\eta^*(\mathrm{eq})^{\frac{1}{4.1}} - \eta^*(t=0)^{\frac{1}{4.1}}} \tag{17}$$

where $\eta^*(t)$ is the complex viscosity as a function of time, $\eta^*(t = 0)$ is the initial complex viscosity at the start of the experiment, and $\eta^*(\mathrm{eq})$ is the final equilibrium viscosity reached under the measuring conditions ($\omega = 1$ rad s^{-1}). The absolute degree of conversion x was then found:

$$x = \frac{[M]_0 + \alpha\cdot\left([M]_{eq} - [M]_0\right)}{[M]_0} \tag{18}$$

where $[M]_0$ is the initial free maleimide concentration, $[M]_{eq}$ is the equilibrium free maleimide concentration at T_a, both estimated from the molecular weight measurements by SEC (Figure 2B). The forward DA rate constant (k_{DA}) and rDA rate constant (k_{rDA}) were determined by fitting the x against time data with eqs 8 and 9, depending on whether the retro or forward reaction was observed, respectively. Using this method, activation energies of 88.8 ± 6.49 and 55.2 ± 4.82 kJ mol^{-1} were obtained for the rDA and DA reactions, respectively (Figure 14A), in excellent agreement with the literature values for other furan maleimide systems [E_a(rDA) = 88 to 102 kJ mol^{-1} and E_a(DA) = 43 to 56 kJ mol^{-1}].[9,67−69,85] This also correlates well with the rDA E_a value found via FTIR in this work (91.7 ± 5.02 kJ mol^{-1}). Interestingly, this procedure remained effective at temperatures below 90 °C, where the equilibrium molecular weight dispersity was substantially higher (Figure 2B) and the relationship described by eq 16 was no longer observed.

K_{eq} for the association reaction was also calculated from the rate constants (k_{DA}/k_{rDA}) which were plotted against reciprocal temperature to construct a van't Hoff plot (Figure 14B). Poor correlation was observed at high temperatures, which suggests that the rate constant extraction procedure was more successful at low temperatures, where the forward DA reaction was monitored. Taking a linear fit of this data allowed the determination of the enthalpy change $\Delta H^\ominus$ and entropy change $\Delta S^\ominus$ of reaction via the van't Hoff equation:

$$\ln K_{eq} = \frac{\Delta S^\ominus}{R} - \frac{\Delta H^\ominus}{R\cdot(T+273)} \tag{19}$$

$\Delta H^\ominus$ and $\Delta S^\ominus$ were calculated from the slope and y intercept, respectively: $\Delta H^\ominus = -52.3 \pm 6.15$ and $\Delta S^\ominus = -147 \pm 18.2$ J K^{-1} mol^{-1}. The obtained values are in reasonable agreement with literature values ($\Delta H^\ominus = -39$ to -60 kJ mol^{-1} and $\Delta S^\ominus = -105$ to -138 J K^{-1} mol).[85−87]

Downloaded from pubs.acs.org/macrobx/article-pdf/doi/10.1021/acs.macromol.6c01484/6895018/ma-2026-014843.pdf by guest on 04 November 2026

https://doi.org/10.1021/acs.macromol.6c01484
Macromolecules XXXX, XXX, XXX−XXX

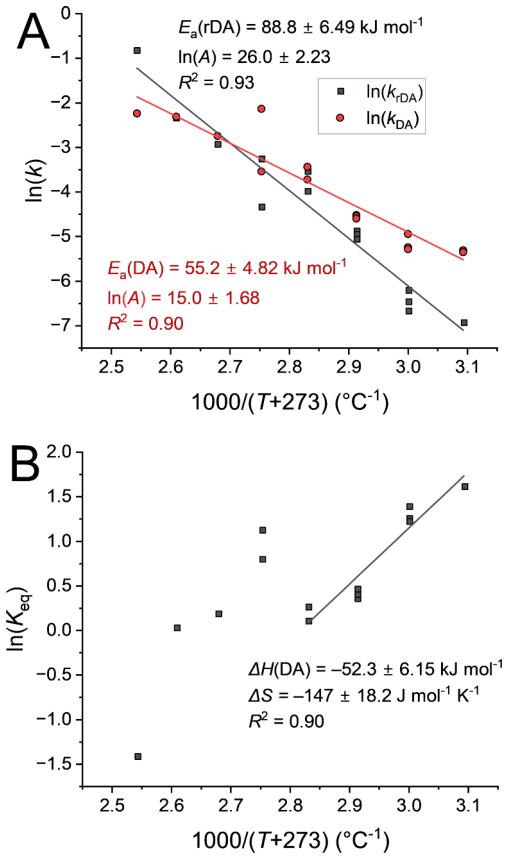


Figure 14. (A) Arrhenius plots of k_{DA} and k_{rDA} rate constants found from rheology time sweeps-the linear fits of the data were used to obtain E_a for the forward and retro DA reaction (red and black lines, respectively) and (B), van't Hoff plot of the forward DA reaction calculated from the rate constants presented in (A).

■ CONCLUSIONS

Linear polyurethane molecules extended with thermoreversible Diels–Alder cycloadducts were prepared and compared to an analogous material containing conventional butanediol chain extender. Owing to their differences in molecular architecture, these materials exhibited substantial differences in physical properties which were investigated in detail.

Analysis of **BDO-PU** suggested a phase separated hard-soft segment morphology, attributed to the use of the short, symmetrical BDO molecule as a chain extender. This was particularly evident in the time-resolved SAXS measurements, which showed that **BDO-PU** exhibited a broad scattering peak in the melt state. This morphology was reflected in its rheological properties, with rubbery plateau behavior observed up to 100 °C due to the presence of a structured melt phase. Construction of a TTS master curve from the frequency sweep data was impossible for **BDO-PU**, probably due to thermorheological complexity arising from a thermally induced phase mixing process which was shown by SAXS (Figures 7C and 12C).

DA-PU was investigated as a more recyclable material due to the reversible dissociation of DA bonds within the polymer backbone. The experimental data showed that **DA-PU** could be dissociated successfully from the reduction in molecular weight after annealing (Figure 2B). The dissociation process also had important consequences, including an increased crystallization rate (Figure 5) and a substantial reduction in melt viscosity (Figure 12A). The SAXS profiles of **DA-PU** recorded at temperatures above the soft segment melting point were featureless, suggesting a homogeneous mixed-phase morphology. This is also supported by the DSC results, which show that **DA-PU** has a slightly higher T_g than **BDO-PU**. This is likely due to the lack of symmetry in the DA cycloadduct used as a chain extender, which produces non-linear, 'kinked' hard segments. In contrast to the behavior observed for **BDO-PU**, the TTS master curve for **DA-PU** showed good empirical agreement, likely as a result of its phase-mixed morphology. The TMWS curve of **DA-PU** was constructed at 80 °C to obtain more information about the effect of molecular weight on viscoelastic behavior, as well as to validate the application of TTS to a material that dissociates. The resulting TMWS master curve was satisfactory and showed good agreement with the TTS master curve, suggesting **DA-PU** has universal viscoelastic behavior with changes in both temperature and molecular weight, despite a significant change in dispersity with temperature. An empirical relationship between M_n and η^*_0 was also established from these experiments. As the fraction of DA bond conversion is directly proportional to M_n, this relationship enabled the development of a procedure for determining DA reaction kinetics from isothermal rheological measurements. The activation energies determined for the forward and retro DA reactions by this method showed excellent agreement with those obtained by FTIR, as well as with values reported in the literature. This validates the use of rheology for measuring reaction kinetics in dissociative polymers, provided the relationship between reaction conversion and viscosity is established experimentally first, and that the material is thermorheologically simple enough that the relationship holds over a range of temperatures. The use of thermally reversible cycloadducts in TPUs provides a major change in thermal properties, morphology and rheology, suggesting a different paradigm in the balance of processing and properties.

■ ASSOCIATED CONTENT

Supporting Information

The Supporting Information is available free of charge at https://pubs.acs.org/doi/10.1021/acs.macromol.6c01484.

Details of PU synthesis and characterization by NMR and FTIR, analysis of intermolecular forces within the PU materials and analysis of Diels–Alder dissociation kinetics by FTIR, as well as analysis of viscoelastic properties of TPUs by rheology (PDF)

■ AUTHOR INFORMATION

Corresponding Authors

Andrew T. Slark – *Chemistry, School of Mathematical and Physical Sciences, University of Sheffield, Dainton Building, Sheffield S3 7HF, U.K.;* orcid.org/0000-0001-7809-0139; Email: a.slark@sheffield.ac.uk

Oleksandr O. Mykhaylyk – *Chemistry, School of Mathematical and Physical Sciences, University of Sheffield, Dainton Building, Sheffield S3 7HF, U.K.;* orcid.org/0000-0003-4110-8328; Email: O.Mykhaylyk@sheffield.ac.uk

Downloaded from pubs.acs.org/macromol/article-pdf/doi/10.1021/acs.macromol.6c01484/6895018/ma-2026-014843.pdf by guest on 04 November 2026

Author

Thomas S. Jackson – *Chemistry, School of Mathematical and Physical Sciences, University of Sheffield, Dainton Building, Sheffield S3 7HF, U.K.*

Complete contact information is available at: https://pubs.acs.org/doi/10.1021/acs.macromol.6c01484

Notes

The authors declare no competing financial interest.

■ ACKNOWLEDGMENTS

A.T.S. and O.O.M. thank EPSRC for a PhD Studentship for T.S.J. (EP/W524360/1). A.T.S. thanks the EPSRC for a Manufacturing Fellowship (EP/R012121/1) and O.O.M. thanks EPSRC for the capital equipment grant to purchase the laboratory-based Xenocs/Excillum SAXS instrument used for characterizing the PU polymers (EP/M028437/1).

■ REFERENCES

(1) *Market volume of polyurethane worldwide from 2015 to 2022, with a forecast for 2023 to 2030*, **2024**. https://www.statista.com/statistics/720341/global-polyurethane-market-size-forecast/#:~:text=The%20global%20market%20volume%20of,million%20metric%20tons%20in%202022 (accessed 02.02.25).

(2) Rossignolo, G.; Malucelli, G.; Lorenzetti, A. Recycling of polyurethanes: where we are and where we are going. *Green Chem.* **2024**, *26* (3), 1132–1152.

(3) Datta, J.; Kopczyńska, P.; Simón, D.; Rodríguez, J. F. Thermo-Chemical Decomposition Study of Polyurethane Elastomer Through Glycerolysis Route with Using Crude and Refined Glycerine as a Transesterification Agent. *J. Polym. Environ.* **2018**, *26* (1), 166–174.

(4) Montarnal, D.; Capelot, M.; Tournilhac, F.; Leibler, L. Silica-Like Malleable Materials from Permanent Organic Networks. *Science* **2011**, *334* (6058), 965–968.

(5) Sridhar, L. M.; Oster, M. O.; Herr, D. E.; Gregg, J. B.; Wilson, J. A.; Slark, A. T. Re-usable thermally reversible crosslinked adhesives from robust polyester and poly (ester urethane) Diels–Alder networks. *Green Chem.* **2020**, *22* (24), 8669–8679.

(6) Turkenburg, D. H.; van Bracht, H.; Funke, B.; Schmider, M.; Janke, D.; Fischer, H. R. Polyurethane adhesives containing Diels–Alder-based thermoreversible bonds. *J. Appl. Polym. Sci.* **2017**, *134* (26), 44972.

(7) Gandini, A. The furan/maleimide Diels–Alder reaction: A versatile click–unclick tool in macromolecular synthesis. *Prog. Polym. Sci.* **2013**, *38* (1), 1–29.

(8) Du, P.; Liu, X.; Zheng, Z.; Wang, X.; Joncheray, T.; Zhang, Y. Synthesis and characterization of linear self-healing polyurethane based on thermally reversible Diels–Alder reaction. *RSC Adv.* **2013**, *3* (35), 15475–15482.

(9) Adzima, B. J.; Aguirre, H. A.; Kloxin, C. J.; Scott, T. F.; Bowman, C. N. Rheological and Chemical Analysis of Reverse Gelation in a Covalently Cross-Linked Diels–Alder Polymer Network. *Macromolecules* **2008**, *41* (23), 9112–9117.

(10) Kloxin, C. J.; Bowman, C. N. Covalent adaptable networks: smart, reconfigurable and responsive network systems. *Chem. Soc. Rev.* **2013**, *42* (17), 7161–7173.

(11) Chen, X.; Dam, M. A.; Ono, K.; Mal, A.; Shen, H.; Nutt, S. R.; Sheran, K.; Wudl, F. A Thermally Re-mendable Cross-Linked Polymeric Material. *Science* **2002**, *295* (5560), 1698–1702.

(12) Murphy, E. B.; Bolanos, E.; Schaffner-Hamann, C.; Wudl, F.; Nutt, S. R.; Auad, M. L. Synthesis and Characterization of a Single-Component Thermally Remendable Polymer Network: Staudinger and Stille Revisited. *Macromolecules* **2008**, *41* (14), 5203–5209.

(13) Craven, J. M.Cross-linked thermally reversible polymers produced from condensation polymers with pendant furan groups cross-linked with maleimides. US US3435003A, **1969**.

(14) Gomez-Lopez, A.; Ayensa, N.; Grignard, B.; Irusta, L.; Calvo, I.; Müller, A. J.; Detrembleur, C.; Sardon, H. Enhanced and Reusable Poly(hydroxy urethane)-Based Low Temperature Hot-Melt Adhesives. *ACS Polym. Au* **2022**, *2* (3), 194–207.

(15) Hyder, M. J.; Godleman, J.; Chippindale, A. M.; Hallett, J. E.; Zinn, T.; Harries, J. L.; Hayes, W. Thermally and Base-Triggered "Debond-on-Demand" Chain-Extended Polyurethane Adhesives. *Macromolecules* **2025**, *58* (1), 681–696.

(16) Hughes, J. C.; Wilson, J. A.; Hawkins, N.; Zhang, Y.; Holland, C.; Slark, A. T. Compatibilisation of immiscible soft segments in self-healing thermoplastic polyurethane elastomers via Diels-Alder cycloaddition. *Eur. Polym. J.* **2025**, *229*, 113881.

(17) Fawcett, S. A. *New Thermally Reversible Thermoplastic Polyurethanes*; Ph.D Thesis,University of Sheffield: Sheffield, UK, **2023**.

(18) Hughes, J. C. *Structure-Property Relationships of Elastomers Containing Thermally Reversible Diels-Alder Bonds*; Ph.D Thesis, University of Sheffield: Sheffield, UK, **2024**.

(19) Pourmohammadi-Mahunaki, M.; Haddadi-Asl, V.; Roghani-Mamaqani, H.; Koosha, M.; Yazdi, M. Effect of chain extender length and molecular architecture on phase separation and rheological properties of ether-based polyurethanes. *Polym. Bull.* **2022**, *79*, 8653–8668.

(20) Tsiotas, A. A. *The role of the chain extender on the phase behaviour and morphology of high hard block content thermoplastic polyurethanes: Thermodynamics-structures-properties*; Ph.D Thesis, The University of Manchester: Manchester, UK, **2012**.

(21) Savelyev, Y. V.; Akhranovich, E. R.; Grekov, A. P.; Privalko, E. G.; Korskanov, V. V.; Shtompel, V. I.; Privalko, V. P.; Pissis, P.; Kanapitsas, A. Influence of chain extenders and chain end groups on properties of segmented polyurethanes. I Phase morphology. *Polymer* **1998**, *39* (15), 3425–3429.

(22) Biemond, G. J. E.; Brasspenning, K.; Gaymans, R. J. Synthesis and selected properties of polyurethanes with monodisperse hard segments based on hexane diisocyanate and three types of chain extenders. *J. Appl. Polym. Sci.* **2012**, *124* (2), 1302–1315.

(23) Chang, Z.; Zhang, M.; Hudson, A. G.; Orler, E. B.; Moore, R. B.; Wilkes, G. L.; Turner, S. R. Synthesis and properties of segmented polyurethanes with triptycene units in the hard segment. *Polymer* **2013**, *54* (26), 6910–6917.

(24) Fawcett, S. A.; Jackson, T. S.; Wilson, J. A.; Hughes, J. C.; Tareq, A. Z.; Hart, L. R.; Hayes, W.; Slark, A. T. The effect of chain extender symmetry, branching and hydrogen bonding capability on the morphology and mechanical properties of thermoplastic polyurethanes. *Polymer* **2026**, *345*, 129578.

(25) Prisacariu, C.; Scortanu, E. Influence of the type of chain extender and urethane group content on the mechanical properties of polyurethane elastomers with flexible hard segments. *High Perform. Polym.* **2011**, *23* (4), 308–313.

(26) Javni, I.; Bilić, O.; Bilić, N.; Petrović, Z. S.; Eastwood, E. A.; Zhang, F.; Ilavský, J. Thermoplastic polyurethanes with isosorbide chain extender. *J. Appl. Polym. Sci.* **2015**, *132* (47), 42830.

(27) Van Bogart, J. W. C.; Gibson, P. E.; Cooper, S. L. Structure-property relationships in polycaprolactone-polyurethanes. *J. Polym. Sci., Polym. Phys. Ed.* **1983**, *21* (1), 65–95.

(28) Yen, M. S.; Cheng, K. L. The effects of soft segments on the physical properties and water vapor permeability of H_{12}MDI-PU cast films. *J. Appl. Polym. Sci.* **1994**, *52* (12), 1707–1717.

(29) Korley, L. T. J.; Pate, B. D.; Thomas, E. L.; Hammond, P. T. Effect of the degree of soft and hard segment ordering on the morphology and mechanical behavior of semicrystalline segmented polyurethanes. *Polymer* **2006**, *47* (9), 3073–3082.

(30) Sonnenschein, M. F.; Lysenko, Z.; Brune, D. A.; Wendt, B. L.; Schrock, A. K. Enhancing polyurethane properties via soft segment crystallization. *Polymer* **2005**, *46* (23), 10158–10166.

Downloaded from pubs.acs.org/macromolbx/article-pdf/doi/10.1021/acs.macromol.6c01484/6895018/ma-2026-014843.pdf by guest on 04 November 2026

(31) Skarja, G. A.; Woodhouse, K. A. Structure-property relationships of degradable polyurethane elastomers containing an amino acid-based chain extender. *J. Appl. Polym. Sci.* **2000**, *75* (12), 1522–1534.
(32) Du, P.; Wu, M.; Liu, X.; Zheng, Z.; Wang, X.; Joncheray, T.; Zhang, Y. Diels–Alder-based crosslinked self-healing polyurethane/urea from polymeric methylene diphenyl diisocyanate. *J. Appl. Polym. Sci.* **2014**, *131* (9), 40234.
(33) Rogers, M. E.; Long, T. E.; Turner, S. R. Introduction to synthetic methods in step-growth polymers. In: *Synthetic Methods in Step-Growth Polymers*, Rogers, M. E.; Long, T. E., Eds.; John Wiley & Sons, Inc., **2003**; pp 1–16.
(34) Hentschel, T.; Münstedt, H. Kinetics of the molar mass decrease in a polyurethane melt: a rheological study. *Polymer* **2001**, *42* (7), 3195–3203.
(35) Yang, W.; Macosko, C.; Wellinghoff, S. Thermal degradation of urethanes based on 4, 4′-diphenylmethane diisocyanate and 1, 4-butanediol (MDI/BDO). *Polymer* **1986**, *27* (8), 1235–1240.
(36) Pal, J.; Sanwaria, S.; Choudhary, A.; Thakur, K.; Nandan, B.; Srivastava, R. K. Thermally Initiated Trans-esterification in Poly(ε-caprolactone) and Its Dependence on Molecular Weight. *J. Polym. Environ.* **2014**, *22* (4), 479–487.
(37) McReynolds, B. T.; Mojtabai, K. D.; Penners, N.; Kim, G.; Lindholm, S.; Lee, Y.; McCoy, J. D.; Chowdhury, S. Understanding the Effect of Side Reactions on the Recyclability of Furan–Maleimide Resins Based on Thermoreversible Diels–Alder Network. *Polymers* **2023**, *15* (5), 1106.
(38) Mark, J. E. In: *Physical properties of polymers*;Springer, **2004**.
(39) Koleske, J. V.; Lundberg, R. D. Lactone polymers. I. Glass transition temperature of poly-ε-caprolactone by means on compatible polymer mixtures. *J. Polym. Sci. A-2: Polym. Phys.* **1969**, *7* (5), 795–807.
(40) Fernández-Tena, A.; Pérez-Camargo, R. A.; Coulembier, O.; Sangroniz, L.; Aranburu, N.; Guerrica-Echevarria, G.; Liu, G.; Wang, D.; Cavallo, D.; Müller, A. J. Effect of Molecular Weight on the Crystallization and Melt Memory of Poly(ε-caprolactone) (PCL). *Macromolecules* **2023**, *56* (12), 4602–4620.
(41) Chen, T. K.; Chui, J. Y.; Shieh, T. S. Glass Transition Behaviors of a Polyurethane Hard Segment based on 4,4′-Diisocyanatodiphenylmethane and 1,4-Butanediol and the Calculation of Microdomain Composition. *Macromolecules* **1997**, *30* (17), 5068–5074.
(42) Wunderlich, B.In: *Macromolecular physics: Crystal Nucleation, Growth, Annealing*;Academic Press, **1976**.
(43) Froidevaux, V.; Borne, M.; Laborbe, E.; Auvergne, R.; Gandini, A.; Boutevin, B. Study of the Diels–Alder and retro-Diels–Alder reaction between furan derivatives and maleimide for the creation of new materials. *RSC Adv.* **2015**, *5* (47), 37742–37754.
(44) Avrami, M. Granulation, Phase Change, and Microstructure Kinetics of Phase Change III. *J. Chem. Phys.* **1941**, *9* (2), 177–184.
(45) Lorenzo, A. T.; Arnal, M. L.; Albuerne, J.; Müller, A. J. DSC isothermal polymer crystallization kinetics measurements and the use of the Avrami equation to fit the data: Guidelines to avoid common problems. *Polym. Test.* **2007**, *26* (2), 222–231.
(46) Jenkins, M. J.; Harrison, K. L. The effect of molecular weight on the crystallization kinetics of polycaprolactone. *Polym. Adv. Technol.* **2006**, *17* (6), 474–478.
(47) Celli, A.; Barbiroli, G.; Berti, C.; Francesco, D. C.; Lorenzetti, C.; Marchese, P.; Marianucci, E. Thermal properties of poly(alkylene dicarboxylate)s derived from 1,12-dodecanedioic acid and even aliphatic diols. *J. Polym. Sci., Part B: Polym. Phys.* **2007**, *45* (9), 1053–1067.
(48) Pérez, R. A.; López, J. V.; Hoskins, J. N.; Zhang, B.; Grayson, S. M.; Casas, M. T.; Puiggalí, J.; Müller, A. J. Nucleation and Antinucleation Effects of Functionalized Carbon Nanotubes on Cyclic and Linear Poly(ε-caprolactones). *Macromolecules* **2014**, *47* (11), 3553–3566.
(49) Pérez-Camargo, R. A.; Liu, G.-M.; Wang, D.-J.; Müller, A. J. Experimental and Data Fitting Guidelines for the Determination of Polymer Crystallization Kinetics. *Chin. J. Polym. Sci.* **2022**, *40* (6), 658–691.
(50) Chatani, Y.; Okita, Y.; Tadokoro, H.; Yamashita, Y. Structural Studies of Polyesters. III Crystal Structure of Poly-ε-caprolactone. *Polym. J.* **1970**, *1* (5), 555–562.
(51) Hu, H.; Dorset, D. L. Crystal structure of poly(iε-caprolactone). *Macromolecules* **1990**, *23* (21), 4604–4607.
(52) Bunn, C. W. The crystal structure of long-chain normal paraffin hydrocarbons. The "shape" of the $>CH_2$ group. *Trans. Faraday Soc.* **1939**, *35*, 482–491.
(53) Miller, J. A.; Lin, S. B.; Hwang, K. K.; Wu, K.; Gibson, P.; Cooper, S. L. Properties of polyether-polyurethane block copolymers: effects of hard segment length distribution. *Macromolecules* **1985**, *18* (1), 32–44.
(54) Zhu, L.; Li, J.; Li, H.; Liu, B.; Chen, J.; Jiang, S. The role of entanglement in crystallization and melting of cyclic poly(ε-caprolactone)s. *CrystEngComm* **2023**, *25* (9), 1383–1392.
(55) Zhu, L.; Li, J.; Li, H.; Liu, B.; Chen, J.; Jiang, S. Crystallization and melting of unentangled poly(ε-caprolactone) cycles containing pendants. *Soft Matter* **2023**, *19* (30), 5795–5804.
(56) Ryan, A. J.; Macosko, C. W.; Bras, W. Order-disorder transition in a block copolyurethane. *Macromolecules* **1992**, *25* (23), 6277–6283.
(57) Merino, D. H.; Feula, A.; Melia, K.; Slark, A. T.; Giannakopoulos, I.; Siviour, C. R.; Buckley, C. P.; Greenland, B. W.; Liu, D.; Gan, Y.; et al. A systematic study of the effect of the hard end-group composition on the microphase separation, thermal and mechanical properties of supramolecular polyurethanes. *Polymer* **2016**, *107*, 368–378.
(58) Yoon, P. J.; Han, C. D. Effect of Thermal History on the Rheological Behavior of Thermoplastic Polyurethanes. *Macromolecules* **2000**, *33* (6), 2171–2183.
(59) Koberstein, J. T.; Galambos, A. F. Multiple melting in segmented polyurethane block copolymers. *Macromolecules* **2002**, *25* (21), 5618–5624.
(60) Li, W.; Ryan, A. J.; Meier, I. K. Effect of Chain Extenders on the Morphology Development in Flexible Polyurethane Foam. *Macromolecules* **2002**, *35* (16), 6306–6312.
(61) Seymour, R. W.; Cooper, S. L. Thermal Analysis of Polyurethane Block Polymers. *Macromolecules* **1973**, *6* (1), 48–53.
(62) Wang, F. C.; Feve, M.; Lam, T. M.; Pascault, J.-P. FTIR analysis of hydrogen bonding in amorphous linear aromatic polyurethanes. I Influence of temperature. *J. Polym. Sci., Part B: Polym. Phys.* **1994**, *32* (8), 1305–1313.
(63) Wang, F. C.; Feve, M.; Lam, T. M.; Pascault, J.-P. FTIR analysis of hydrogen bonding in amorphous linear aromatic polyurethanes. II Influence of styrene solvent. *J. Polym. Sci., Part B: Polym. Phys.* **1994**, *32* (8), 1315–1320.
(64) Coleman, M. M.; Lee, K. H.; Skrovanek, D. J.; Painter, P. C. Hydrogen bonding in polymers. 4 Infrared temperature studies of a simple polyurethane. *Macromolecules* **1986**, *19* (8), 2149–2157.
(65) Decker, C.; Bianchi, C.; Jönsson, S. Light-induced crosslinking polymerization of a novel N-substituted bis-maleimide monomer. *Polymer* **2004**, *45* (17), 5803–5811.
(66) Parker, S. F. Vibrational spectroscopy of N-methylmaleimide. *Spectrochim. Acta, Part A* **1995**, *51* (12), 2067–2072.
(67) Carneiro de Oliveira, J.; Laborie, M.-P.; Roucoules, V. Thermodynamic and Kinetic Study of Diels–Alder Reaction between Furfuryl Alcohol and N-Hydroxymaleimides—An Assessment for Materials Application. *Molecules* **2020**, *25* (2), 243.
(68) Ručigaj, A.; Kobal, T.; Šebenik, U.; Krajnc, M. Kinetic model of a Diels–Alder reaction in a molten state: thermal and viscoelastic behaviour. *Polym. Bull.* **2020**, *77* (3), 1377–1397.
(69) Stirn, Z.; Rucigaj, A.; Krajnc, M. Characterization and kinetic study of Diels-Alder reaction: Detailed study on N-phenylmaleimide and furan based benzoxazine with potential self-healing application. *Express Polym. Lett.* **2016**, *10*, 537–547.
(70) Heydarnezhad, H. R.; Mohammadi, N.; Arbe, A.; Alegria, A. How Does Microstructural Design Affect the Dynamics and Rheology of Segmented Polyurethanes? *Macromolecules* **2020**, *53* (13), 5381–5398.
(71) Han, C. D.; Jhon, M. S. Correlations of the first normal stress difference with shear stress and of the storage modulus with loss modulus for homopolymers. *J. Appl. Polym. Sci.* **1986**, *32* (3), 3809–3840.
(72) Velankar, S.; Cooper, S. L. Microphase Separation and Rheological Properties of Polyurethane Melts. 1 Effect of Block Length. *Macromolecules* **1998**, *31* (26), 9181–9192.

Downloaded from pubs.acs.org/macromolbx/article-pdf/doi/10.1021/acs.macromol.6c01484/6895801/8/ma-2026-014843.pdf by guest on 04 November 2026

(73) Velankar, S.; Cooper, S. L. Microphase Separation and Rheological Properties of Polyurethane Melts. 3 Effect of Block Incompatibility on the Viscoelastic Properties. *Macromolecules* **2000**, *33* (2), 395–403.
(74) Noroozi, N.; Thomson, J. A.; Noroozi, N.; Schafer, L. L.; Hatzikiriakos, S. G. Viscoelastic behaviour and flow instabilities of biodegradable poly (ε-caprolactone) polyesters. *Rheol. Acta* **2012**, *51* (2), 179–192.
(75) Berzin, F.; Vergnes, B. Time/Molecular Weight Superposition to Describe the Behavior of Controlled-Rheology Polypropylenes. *Polymers* **2022**, *14* (16), 3398.
(76) Ferry, J. D. *Viscoelastic properties of polymers*; John Wiley & Sons, **1980**.
(77) Vinogradov, G. V.; Ya. Malkin, A. Rheological properties of polymer melts. *J. Polym. Sci. A-2: Polym. Phys.* **1966**, *4* (1), 135–154.
(78) Minoshima, W.; White, J. L.; Spruiell, J. E. Experimental investigation of the influence of molecular weight distribution on the rheological properties of polypropylene melts. *Polym. Eng. Sci.* **1980**, *20* (17), 1166–1176.
(79) Han, C. D. In: *Rheology and processing of polymeric materials: Volume 1: Polymer Rheology*;Oxford University Press, **2007**.
(80) Likhtman, A. E.; McLeish, T. C. B. Quantitative Theory for Linear Dynamics of Linear Entangled Polymers. *Macromolecules* **2002**, *35* (16), 6332–6343.
(81) Graessley, W. W. Some phenomenological consequences of the Doi–Edwards theory of viscoelasticity. *J. Polym. Sci., Polym. Phys. Ed.* **1980**, *18* (1), 27–34.
(82) Choi, S.; Han, C. D. Molecular Weight Dependence of Zero-Shear Viscosity of Block Copolymers in the Disordered State. *Macromolecules* **2004**, *37* (1), 215–225.
(83) Berne, D.; Laviéville, S.; Leclerc, E.; Caillol, S.; Ladmiral, V.; Bakkali-Hassani, C. How to Characterize Covalent Adaptable Networks: A User Guide. *ACS Polym. Au* **2025**, *5* (3), 214–240.
(84) Barzycki, D. C.; Ezzeddine, D.; Shanbhag, S.; Ricarte, R. G. Linear Viscoelasticity of Polystyrene Vitrimers: Segmental Motions and the Slow Arrhenius Process. *Macromolecules* **2025**, *58* (8), 3949–3963.
(85) Scheltjens, G.; Diaz, M. M.; Brancart, J.; Van Assche, G.; Van Mele, B. A self-healing polymer network based on reversible covalent bonding. *React. Funct. Polym.* **2013**, *73* (2), 413–420.
(86) Sheridan, R. J.; Bowman, C. N. A Simple Relationship Relating Linear Viscoelastic Properties and Chemical Structure in a Model Diels–Alder Polymer Network. *Macromolecules* **2012**, *45* (18), 7634–7641.
(87) Diaz, M. M.; Van Assche, G.; Maurer, F. H. J.; Van Mele, B. Thermophysical characterization of a reversible dynamic polymer network based on kinetics and equilibrium of an amorphous furan-maleimide Diels-Alder cycloaddition. *Polymer* **2017**, *120*, 176–188.

Downloaded from pubs.acs.org/mamobx/article-pdf/doi/10.1021/acs.macromol.6c01484/6895018/ma-2026-014843.pdf by guest on 04 November 2026

https://doi.org/10.1021/acs.macromol.6c01484
Macromolecules XXXX, XXX, XXX–XXX